



# General anesthetics activate a potent central pain-suppression circuit in the amygdala

Thuy Hua<sup>1,3</sup> , Bin Chen<sup>1,3</sup> , Dongye Lu<sup>1</sup>, Katsuyasu Sakurai<sup>1</sup>, Shengli Zhao<sup>1</sup>, Bao-Xia Han<sup>1</sup>, Jiwoo Kim<sup>1</sup>, Luping Yin<sup>1</sup> , Yong Chen<sup>2</sup>, Jinghao Lu<sup>1</sup> and Fan Wang<sup>1</sup>  

**General anesthesia (GA) can produce analgesia (loss of pain) independent of inducing loss of consciousness, but the underlying mechanisms remain unclear. We hypothesized that GA suppresses pain in part by activating supraspinal analgesic circuits. We discovered a distinct population of GABAergic neurons activated by GA in the mouse central amygdala (CeA<sub>GA</sub> neurons). In vivo calcium imaging revealed that different GA drugs activate a shared ensemble of CeA<sub>GA</sub> neurons. CeA<sub>GA</sub> neurons also possess basal activity that mostly reflects animals' internal state rather than external stimuli. Optogenetic activation of CeA<sub>GA</sub> potently suppressed both pain-elicited reflexive and self-recuperating behaviors across sensory modalities and abolished neuropathic pain-induced mechanical (hyper-)sensitivity. Conversely, inhibition of CeA<sub>GA</sub> activity exacerbated pain, produced strong aversion and canceled the analgesic effect of low-dose ketamine. CeA<sub>GA</sub> neurons have widespread inhibitory projections to many affective pain-processing centers. Our study points to CeA<sub>GA</sub> as a potential powerful therapeutic target for alleviating chronic pain.**

One of the main effects of GA is analgesia, or loss of pain perception, which is critical for making surgery and other invasive medical procedures more humane. Although GA is well known to induce loss of consciousness, it is often assumed that analgesia is a consequence of the unconscious brain that cannot perceive pain. However, many cases of intraoperative awareness in which patients were aware of surgeons' conversations and other events in the operating room but nevertheless did not feel pain suggest that there could be a specific analgesic pathway that is independent of the loss-of-consciousness effects of GA drugs<sup>1,2</sup>. Furthermore, ketamine, a commonly used GA drug, at low sub-anesthetic dose, is used by anesthesiologists as an analgesic without inducing unconsciousness and with minimal physiological effects<sup>3-5</sup>. Previously, it was thought that low-dose GA drugs induce analgesia through blocking peripheral nociceptive transmission in the dorsal horn of the spinal cord; however, patients treated in this manner can still perceive stimuli in the absence of pain, which is not consistent with this idea<sup>3,6</sup>. These observations suggest that low-dose GA analgesia might act at levels above the spinal cord (supraspinal centers) that dissociate pain perception from the detection of noxious sensory stimuli. The locations of such centers and identities of such neurons remain unknown. We hypothesized that GA-induced analgesia involves activation of a specific central pain-suppression circuit. In this study, we tested our hypothesis and discovered that GA indeed activates a distinct population of GABAergic neurons in the CeA. We further discovered that these cells have profound analgesic effects that suppress both the sensory and affective aspects of pain processing in both naïve animals and in models of acute and chronic neuropathic pain and are required for the pain-relieving effect of low-dose ketamine.

## Results

**Identification of CeA<sub>GA</sub> neurons that are activated by isoflurane and ketamine anesthetics.** To begin to test our hypothesis, we used the immediate early gene Fos (encoded by the *c-fos* gene) as a marker for recently activated neurons and searched for neurons

that remained strongly Fos<sup>+</sup> after exposure to 2 h of isoflurane and oxygen GA (exposure to oxygen alone was used as controls). This experiment revealed three clusters of Fos<sup>+</sup> neurons under isoflurane but not oxygen: one in the CeA, one in the oval division of the bed nucleus of the stria terminalis (ovBNST) and one in the supraoptic nucleus (SON) (Fig. 1a and Extended Data Fig. 1a–c). We recently showed that the GA-activated SON neurons promote slow-wave sleep and extend GA duration (i.e. this cluster of cells is related to the sedative aspects of GA)<sup>7</sup>. The functions of GA-activated ovBNST neurons are not yet known. Here we focused on GA-activated Fos<sup>+</sup> cells in the CeA (Fig. 1a).

Notably, similar to isoflurane, intraperitoneal (i.p.) administration of ketamine and xylazine (K/X) (but not saline control) also induced Fos<sup>+</sup> expression in a subset of CeA cells (Fig. 1a), hereafter referred to as CeA<sub>GA</sub> neurons. This observation initially came as a surprise, because CeA is well known to be activated by painful stimuli and plays important functions in processing fear and pain<sup>8-12</sup>. Furthermore, CeA is known to contain molecularly and functionally heterogeneous populations of neurons<sup>8,9,13</sup>. We therefore first characterized CeA<sub>GA</sub> cells using several molecular markers. Exposing vGat-Cre::Rosa-stop-GFP mice, in which all GABAergic cells are labeled with GFP, to isoflurane GA, revealed that CeA<sub>GA</sub> neurons are all GABAergic cells (Extended Data Fig. 1d). Using two-color fluorescence in situ hybridization or two-color immunofluorescence, we found that CeA<sub>GA</sub> neurons largely do not overlap with neurons expressing somatostatin (*Sst*), prodynorphin (*Pdyn*), neurotensin (*Nts*) or CGRP-receptor (*Calcrl*) (Extended Data Fig. 1e–i). Although we did not observe any candidate genes that were specifically expressed by all CeA<sub>GA</sub> neurons, we discovered that some of these cells coexpress pre-enkephalin (*Penk*; here we use the commonly adopted name *Penk1*) or protein kinase C (PKC)-[delta] (*Prkcd*; here we use the commonly adopted name *Pkc-d*); however, only a subset of the total neurons expressing *Penk1* or *Pkc-d* were Fos<sup>+</sup> CeA<sub>GA</sub> neurons. Specifically, using a three-color hybridization chain reaction (HCR) in situ hybridization method<sup>10</sup>, we found that *Penk1* was widely expressed by cells both in the CeA and in

<sup>1</sup>Department of Neurobiology, Duke University Medical Center, Durham, NC, USA. <sup>2</sup>Department of Neurology, Duke University Medical Center, Durham, NC, USA. <sup>3</sup>These authors contributed equally: Thuy Hua, Bin Chen. ✉e-mail: [thuy.hua@duke.edu](mailto:thuy.hua@duke.edu); [fan.wang@duke.edu](mailto:fan.wang@duke.edu)

nearby striatum and extended amygdala. *Pkc-d*-expressing neurons located in the anterior and medial part of the CeA did not overlap with CeA<sub>GA</sub> neurons, whereas in the posterior part of the CeA, they partially overlapped with CeA<sub>GA</sub> neurons (Fig. 1c). Collectively, of the total CeA<sub>GA</sub> neurons,  $51.9 \pm 7.8\%$  expressed *Penk1*, whereas  $79.2 \pm 12.6\%$  expressed *Pkc-d* (Fig. 1f (i,ii)). Of the total cells expressing *Pkc-d*,  $61.5 \pm 14.5\%$  were isoflurane-induced Fos<sup>+</sup> cells (Fig. 1f (iii)). The partial overlap of *Penk1*- or *Pkc-d*-expressing cells with CeA<sub>GA</sub> indicated that GA activated a heterogeneous population of CeA cells.

**Selective capturing of isoflurane-activated CeA<sub>GA</sub> neurons using CANE revealed a shared ensemble of GA-activated neurons in CeA.** Because we did not identify any molecular marker genes that can be used to specifically label all CeA<sub>GA</sub> cells, we sought to label and manipulate them using a Fos-based viral-genetic method (Capturing Activated Neuronal Ensembles (CANE))<sup>11,12</sup>. CANE uses Fos<sup>TVA</sup> knock-in mice and engineered viruses (CANE-lentivirus (CANE-LV)) to express desired transgenes in Fos<sup>+</sup> cells. The selectivity and efficiency of CANE-capturing CeA<sub>GA</sub> was determined through a two-bout anesthesia paradigm (Fig. 1b). First, we co-injected CANE-LV-Cre and AAV-Flex-GFP into the CeA at 2 h after isoflurane GA induction to express GFP in CeA<sub>GA</sub> neurons (Fig. 1b,d,e). Second, 3 weeks later, the same animals were re-exposed to isoflurane GA and sacrificed for Fos immunostaining (Fig. 1e). Note that previous studies revealed certain lateralization of CeA<sup>14–16</sup>. However, we found that isoflurane GA activated a similar number of neurons with similar cell body sizes in both the left and right CeA (Fig. 1i), and we could use CANE to label CeA<sub>GA</sub> neurons equally well on both sides (one representative example mouse is shown in Fig. 1d). Furthermore, serial sections through the fore-brain revealed selective capturing of CeA<sub>GA</sub> cells without ectopic labeling in the nearby basolateral amygdala or along the injection path (Fig. 1d). On average,  $71.0 \pm 18.3\%$  of the total Fos<sup>+</sup> cells were CANE<sub>ISO</sub>-GFP<sup>+</sup> ( $n = 4$  mice), and  $77.60 \pm 6.5\%$  CANE<sub>ISO</sub>-GFP<sup>+</sup> cells re-expressed Fos from the second exposure to isoflurane ( $n = 5$  mice) (Fig. 1h). This result indicated that CANE is sufficiently specific and efficient at capturing CeA<sub>GA</sub> neurons.

Next, we asked whether CANE-labeled isoflurane-activated neurons could induce Fos by other anesthetics. We exposed mice labeled with CANE<sub>ISO</sub>-GFP to either K/X ( $n = 4$ ) or dexmedetomidine (Dex) ( $n = 4$ ) anesthesia. Approximately  $39.0 \pm 7.1\%$  and  $51.0 \pm 8.1\%$  of CANE<sub>ISO</sub>-GFP<sup>+</sup> cells re-expressed Fos in response to K/X or Dex, respectively (Fig. 1g,h), suggesting that there is a shared ensemble of CeA neurons activated by different GA drugs. Because isoflurane reliably induces Fos<sup>+</sup> in the largest population of CeA neurons, we therefore, in all subsequent experiments, used CANE in conjunction with isoflurane anesthesia to capture CeA<sub>GA</sub> neurons.

**In vivo imaging of CeA<sub>GA</sub> neurons in responses to isoflurane or ketamine anesthesia.** To characterize the in vivo activity of CeA<sub>GA</sub> neurons during GA induction and maintenance in freely moving mice, we performed in vivo calcium imaging experiments. We used CANE to express the calcium indicator GCaMP6m in CeA<sub>GA</sub> neurons by co-injecting CANE-LV-Cre and AAV2/1-CAG-Flex-GCaMP6m into the CeA of Fos<sup>TVA</sup> mice after 2 h of isoflurane GA (Fig. 2a and Extended Data Fig. 2a). Subsequently, we recorded the calcium dynamics of these cells when we re-exposed mice to isoflurane using a gradient refractive index (GRIN) lens coupled to a miniaturized integrated fluorescence microscope and processed using the MINIPIPE method<sup>17</sup> (Fig. 2a, left). Importantly, re-exposure of isoflurane activated many CANE-GCaMP6m-captured CeA<sub>GA</sub> neurons (Fig. 2b and Supplementary Video 1). To characterize the activity patterns, we sorted neurons based on the ratio of an individual neuron's mean fluorescence during isoflurane exposure (0–20 min) to its baseline (awake state, –4 to 0 min) (583 neurons, Fig. 2c). This analysis revealed that, during isoflurane GA, 89.7% (523/583) of imaged neurons exhibited increased fluorescence (isoflurane-active neurons, cyan rectangle in Fig. 2c), whereas a much smaller minority (10.3%, 60/583) showed decreased fluorescence (isoflurane-suppressed neurons, yellow rectangle in Fig. 2c). The small number of isoflurane-suppressed cells might be the result of nonspecific labeling due to background Fos expression at the time of CANE capturing.

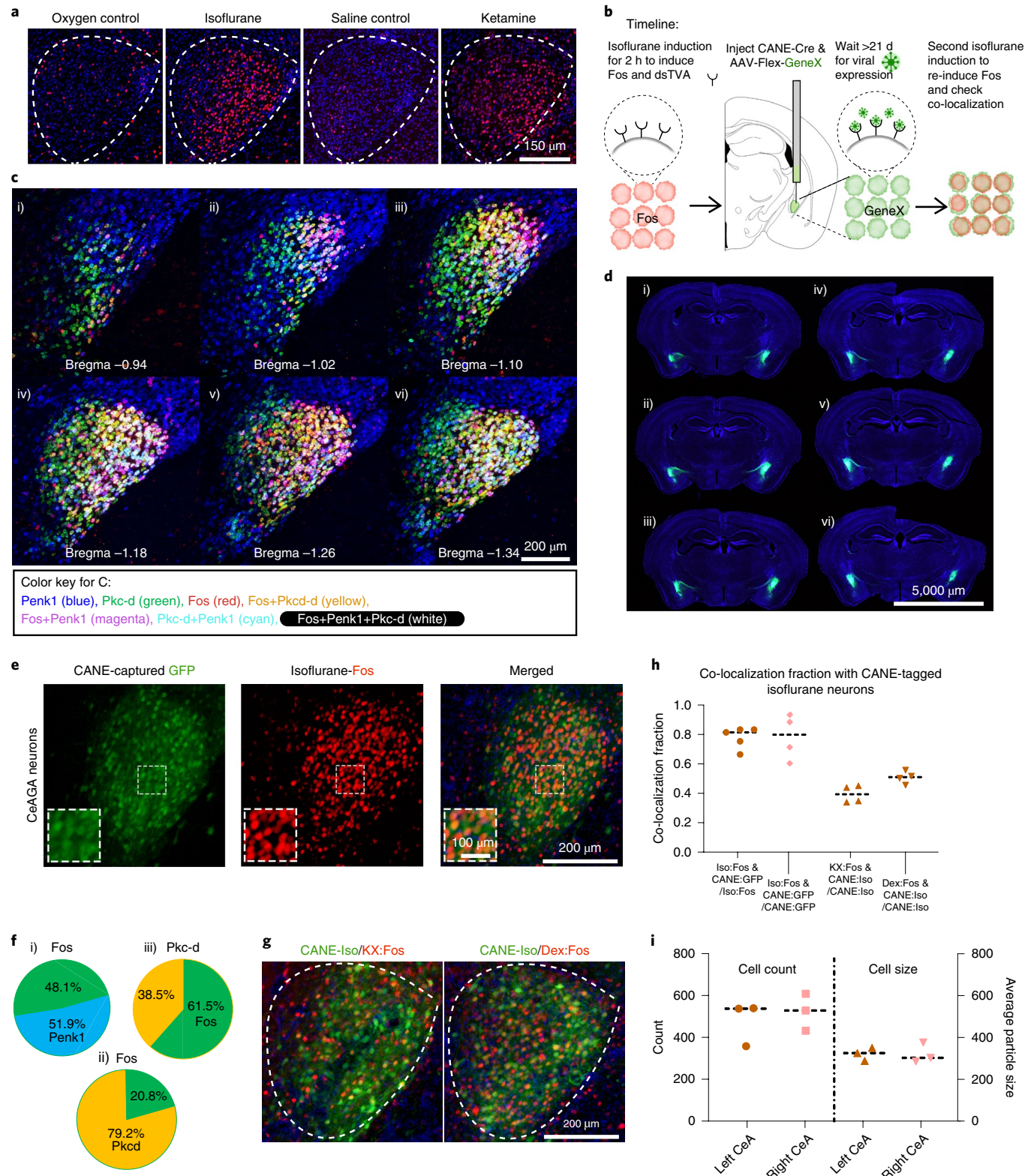
Among the isoflurane-active neurons, we found subsets of neurons that had very low baseline activity but were significantly activated by isoflurane (neurons located at the top of the sorted heat map in Fig. 2c), whereas other subsets had spontaneous baseline activity and were further activated after isoflurane exposure. We re-sorted the neurons by comparing their mean activity during the last 10 min (10–20 min) of isoflurane exposure to those during the first 10 min (0–10 min) (Fig. 2d). This comparison revealed two subpopulations: 11.8% (69/583) of neurons showed persistent firing during the whole GA process (isoflurane-sustained neurons, red rectangle in Fig. 2d), and 77.9% (454/583) of neurons showed transient firing (with increased activity only at 0–10 min of isoflurane exposure, isoflurane-transient neurons, orange rectangle in Fig. 2d). This result suggested that transient activation by isoflurane was sufficient to induce and/or maintain Fos expression in CeA<sub>GA</sub> neurons that enabled CANE-based capturing of these cells. We later tested whether low-concentration isoflurane (0.5%) would result in more persistently activated neurons. All 12 imaged mice contained both sustained and transient isoflurane-active neurons across different imaging sessions (Extended Data Fig. 2d). In addition, we also applied several different quantitative analysis methods (Methods) to further characterize CeA<sub>GA</sub> responses across individuals and across anesthesia sessions. All analyses revealed that most CANE<sub>ISO</sub>-GCaMP6m-captured CeA<sub>GA</sub> neurons were reactivated

**Fig. 1 | Ensembles of neurons in the CeA are activated by GA.** **a**, Representative images of Fos<sup>+</sup> neurons in the CeA from exposure to oxygen control, isoflurane, saline control and K/X injection. Repeated experiments for  $n = 3$  biologically independent samples. **b**, Schematic of CANE capturing of Fos<sup>+</sup> CeA<sub>GA</sub> neurons, followed by a second exposure to isoflurane GA to re-induce Fos. **c**, Representative images of three-color hybridization chain reaction experiments examining the expression of *Penk1* and *Pkc-d* with Fos<sup>+</sup> CeA<sub>GA</sub> neurons (induced by isoflurane). Bregma, –0.94 mm to –1.34 mm. Repeated experiments for  $n = 3$  biologically independent samples. **d**, Six sequential coronal brain sections from one representative mouse containing bilateral CeA<sub>GA</sub> captured neurons (CANE<sub>ISO</sub>-GFP). Repeated experiments for  $n = 5$  biologically independent samples. **e**, Representative images of captured CeA<sub>GA</sub> neurons (green, GFP) from first isoflurane exposure, Fos<sup>+</sup> activation from second isoflurane exposure (red) and their merged image showing co-localization (orange cells). Repeated experiments for  $n = 5$  biologically independent samples. **f** (i,ii), Percentage of *Penk1* and *Pkc-d* overlap over Fos<sup>+</sup> CeA<sub>GA</sub> neurons and (iii) Fos<sup>+</sup> CeA<sub>GA</sub> neurons over total *Pkc-d* neurons ( $n = 3$  biologically independent samples). **g**, Representative images of CANE<sub>GFP</sub> captured CeA<sub>GA</sub> neurons versus Fos<sup>+</sup> neurons in the CeA induced by K/X and Dex. Repeated experiments for  $n = 4$  biologically independent samples. **h**, Quantification of the fraction of Fos<sup>+</sup> neurons induced by isoflurane ( $0.776 \pm 0.065$ ), K/X ( $0.390 \pm 0.051$ ) and Dex ( $0.505 \pm 0.036$ ) over the total Fos<sup>+</sup> CeA<sub>GA</sub> neurons (induced by isoflurane) and CANE<sub>ISO</sub>-GFP over isoflurane-induced Fos<sup>+</sup> neurons ( $0.780 \pm 0.132$ ) ( $n = 4$  biologically independent samples). **i**, Quantification of averaged Fos<sup>+</sup> CeA<sub>GA</sub> neurons in the left ( $486.33 \pm 77.31$ ) and right ( $527 \pm 65.82$ ) CeA and their respective average particle size ( $321.62 \pm 23.26$ , left, and  $321.86 \pm 35.75$ , right) ( $n = 3$  biologically independent samples). Numbers represent the sums of cell counts from six serial 80- $\mu$ m sections containing CeA (but only a single focal plane (6  $\mu$ m) per section was counted).

by isoflurane (Extended Data Fig. 2f). Note that the heterogeneous activity pattern of CeA<sub>GA</sub> neurons was consistent with the heterogeneity revealed by our molecular characterizations (that is, partial overlap with *Penk1* and *Pkc-d*, Fig. 1c,f).

We next asked whether the CANE-GCaMP6m-captured isoflurane-active neurons could also respond to K/X-induced GA (ketamine, 100 mg kg<sup>-1</sup>, and xylazine, 10 mg kg<sup>-1</sup>) in vivo. We

found that 89.4% of CANE<sub>ISO</sub>-GCaMP6m neurons had increased calcium signals after K/X injection (304/340 were ketamine-active neurons and 36/340 were ketamine-suppressed neurons, Fig. 2e). Ketamine-active neurons also showed either persistent (23.2%, 79/340 neurons) or transient (66.2%, 225/340 neurons) activation after ketamine administration (Fig. 2f). The percentages of ketamine transiently versus ketamine sustainably activated neurons



from individual mice are shown (Extended Data Fig. 2e). Additional characterizations using other quantitative methods showed the distributions of ketamine-responsive CeA<sub>GA</sub> neurons on the basis of these different measurements (Extended Data Fig. 2g).

Furthermore, using a previously described method for registering images and tracking cells across days<sup>18</sup> with some modifications (Methods), we managed to track 160 neurons (captured using CANE<sub>ISO</sub>-GCaMP6m) between isoflurane-GA and ketamine-GA imaging sessions (same cells across days from nine mice, Fig. 2g). We found that 88.15% (119/135) of tracked isoflurane-activated neurons were also activated by ketamine (Fig. 2h) using the criterion applied in Fig. 2c,e. When analyzing the activity profiles of these 160 neurons using other methods and criteria (Methods), even with the most stringent criteria, we still found that 57% of isoflurane-activated neurons were also activated by ketamine (Fig. 2h, right). Note that the percentage of dual-activated neurons obtained with calcium imaging was higher than that obtained using Fos staining (Fig. 1h,g), perhaps owing to the fact that neuronal firing does not always lead to Fos expression. Taken together, these *in vivo* imaging results strongly support the existence of a shared ensemble of CeA<sub>GA</sub> neurons that can be activated by both isoflurane and ketamine GA.

**Activity of most CeA<sub>GA</sub> neurons is suppressed by stress.** The transient activation of subsets of CeA<sub>GA</sub> neurons upon isoflurane infusion or ketamine administration raised the question of whether such activities are stress responses. To test this, we subjected mice for 90 min of restraint stress. Stress strongly induced Fos expression in the basolateral amygdala (BLA) but only moderately activated Fos in the CeA (Extended Data Fig. 3b). We next captured CeA<sub>GA</sub> neurons with CANE-tdTomato and subsequently subjected the same mice to 90 min of restraint stress (Extended Data Fig. 3a). We found that only 12 ± 2% of CeA<sub>GA</sub>-tdTomato neurons co-localized with Fos<sup>+</sup> stress-activated neurons, and 27 ± 2% of stress-activated neurons co-localized with CeA<sub>GA</sub>-tdTomato neurons (*n* = 3, Extended Data Fig. 3b). We further imaged the *in vivo* calcium activity of CANE<sub>ISO</sub>-GCaMP6m-captured CeA<sub>GA</sub> neurons in response to restraint stress (282 neurons, Extended Data Fig. 3a). Activity of most CANE<sub>ISO</sub>-GCaMP6m neurons was suppressed during restraint, with only a small number of cells exhibiting stress-induced activation (Extended Data Fig. 3c,d). Furthermore, because CANE captured cells containing a small proportion of isoflurane-suppressed neurons, to further characterize the stress responses, we also applied same-cell tracking<sup>18</sup> and identified neurons that were imaged during both isoflurane-GA and restraint

stress sessions (we tracked 172 same neurons). Using two different measures to categorize their responses to isoflurane (Methods), we confirmed that most isoflurane-activated CeA<sub>GA</sub> neurons were inhibited by stress (Extended Data Fig. 3e–h).

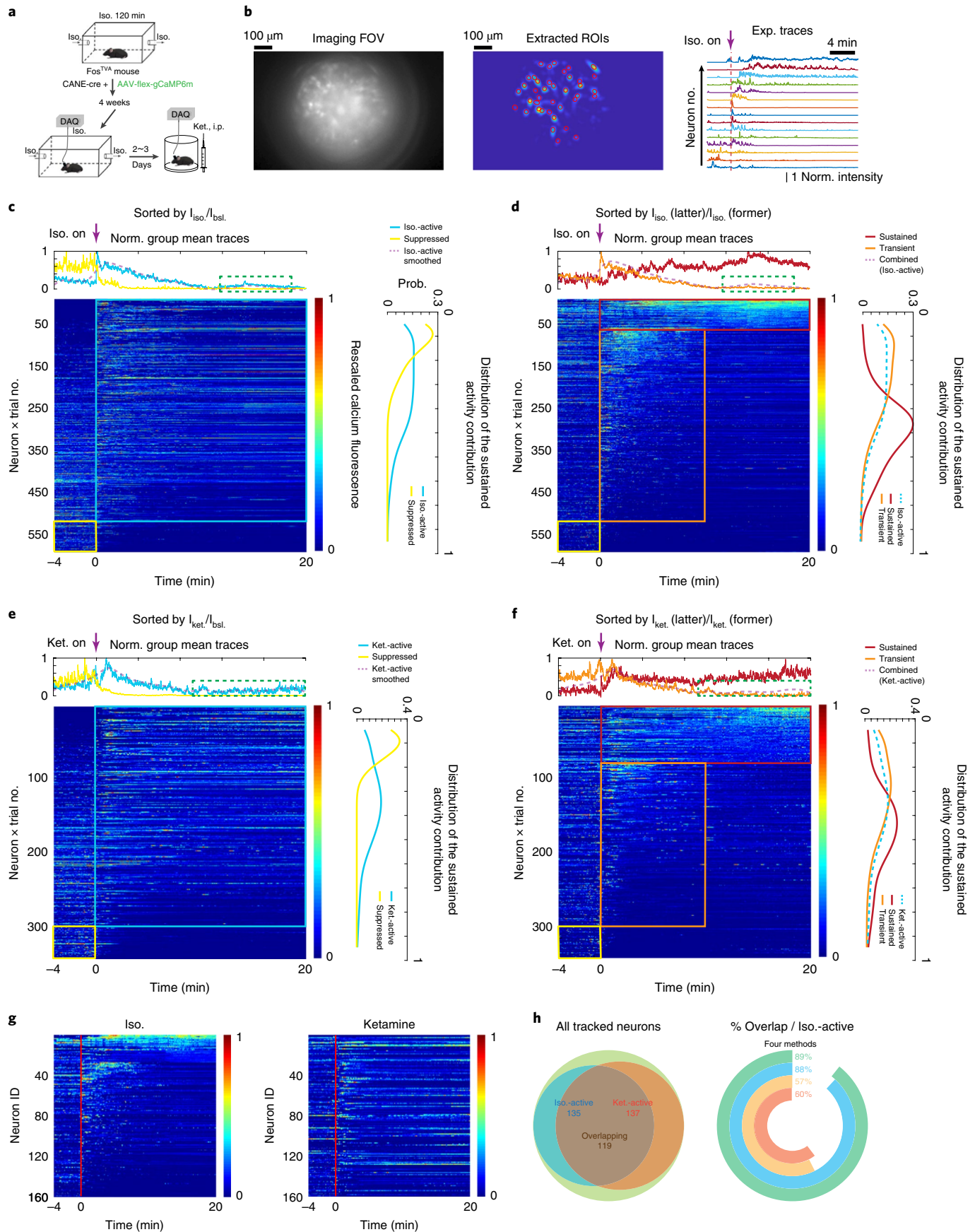
**Optogenetic manipulation of CeA<sub>GA</sub> neurons did not induce fear-like behaviors or change the gross brain state.** Because CeA is generally known as a key center in the fear circuit, we examined whether activation of CeA<sub>GA</sub> neurons induced anxiety- and fear-like behavior. To do this, we expressed either the optogenetic neuronal activator channelrhodopsin<sup>19</sup> (CeA<sub>GA</sub>-ChR2) or the optogenetic silencer enhanced archaerhodopsin 3.0 (ref. <sup>20</sup>) (CeA<sub>GA</sub>-eArch) in CeA<sub>GA</sub> cells using CANE (after 2 h of isoflurane; examples of post hoc fiber tracts are shown in Extended Data Fig. 2c). Mice with CANE-mediated GFP expression in CeA<sub>GA</sub> neurons (CeA<sub>GA</sub>-GFP) were used as controls. We subjected CeA<sub>GA</sub>-GFP, CeA<sub>GA</sub>-ChR2 and CeA<sub>GA</sub>-eArch mice to the open field test and the elevated plus maze (EPM) test with or without photo-illumination. Neither optogenetic activation nor inhibition of CeA<sub>GA</sub> neurons induced any fear-like freezing or fleeing or cornering behaviors in the open field (Supplementary Video 2 and Extended Data Fig. 4a,b) or changed the mouse's behavior in the EPM (Extended Data Fig. 4a,c,d). Specifically, optogenetic manipulation of CeA<sub>GA</sub> neurons did not increase the time that animals spent in the outer perimeter of the open field or in the closed arm of the EPM (Extended Data Fig. 4b,d). We further examined whether activation of CeA<sub>GA</sub> neurons altered the gross brain state by comparing electroencephalogram (EEG) recorded in the frontal and parietal cortex in the absence or presence of optogenetic activation of CeA<sub>GA</sub> neurons in CeA<sub>GA</sub>-ChR2 mice (*n* = 3). The results showed that activating CeA<sub>GA</sub> neurons has no observable effects on the EEG power spectrums (Extended Data Fig. 4e,f).

**Optogenetic activation or silencing of CeA<sub>GA</sub> neurons bidirectionally and potently altered nocifensive reflexes across sensory modalities.** Next, we asked whether these CeA<sub>GA</sub> neurons play a role in regulating nociception sensitivity in naïve mice. We subjected the three groups of mice (CeA<sub>GA</sub>-GFP control, CeA<sub>GA</sub>-ChR2 and CeA<sub>GA</sub>-eArch) to a battery of commonly used mechanical, thermal or cold sensory tests. For mechanical sensitivity, a range of von Frey filaments (0.008–1.0 g) or an electronic von Frey device (50 g per 5 s) was used to stimulate either the face (with all whiskers intact) (Fig. 3a) or the hind paw, respectively. We assessed the reflexive withdrawal responses to stimuli applied to the left or right side (in randomized order for different animals) with or without

**Fig. 2 | Activity patterns of CANE<sub>ISO</sub>-GCaMP6m-captured CeA<sub>GA</sub> neurons during isoflurane and ketamine GA.** **a**, Calcium imaging recording of CANE<sub>ISO</sub>-GCaMP6m-captured CeA<sub>GA</sub> neurons during isoflurane- or ketamine-induced GA. **b**, Left: an example frame from the raw calcium imaging video. Middle: extracted ROI footprints superimposed on the maximum intensity projection. Right: normalized calcium fluorescence traces of the neurons during isoflurane-induced GA. Norm. intensity, normalized calcium signals rescaled to 0–1. FOV, field of view. **c**, Activity patterns of CANE<sub>ISO</sub>-GCaMP6m-captured CeA<sub>GA</sub> neurons sorted by the ratio of the individual neuron's mean activity during isoflurane exposure (0–20 min) to its baseline activity (awake state, –4 to 0 min). Cyan and yellow rectangle indicates isoflurane-active and isoflurane-suppressed neurons separately. Top: the average fluorescence traces of each group of neurons. Right: distribution of contributions to the sustained activity from each group of neurons. Green dashed rectangle indicates a subgroup of isoflurane-active neurons remaining activated under anesthesia. **d**, Two subpopulations of isoflurane-active neurons sorted by the ratio of an individual neuron's mean activity during the last 10 min (10–20 min) of isoflurane exposure to its first 10 min (0–10 min). Red and orange rectangles indicate isoflurane-sustained and isoflurane-transient neurons separately. **e**, Activity patterns of CANE<sub>ISO</sub>-GCaMP6m-captured CeA<sub>GA</sub> neurons in responses to ketamine injected by the ratio of an individual neuron's mean activity after ketamine injection to its baseline activity. Cyan and yellow rectangles indicate ketamine-active and ketamine-suppressed neurons, respectively. **f**, Two subpopulations of ketamine-active neurons sorted by the ratio of an individual neuron's mean activity during the last 10 min of ketamine to its first 10 min. Red and orange rectangles indicate ketamine-sustained and ketamine-transient neurons separately. Arrows indicate the time when isoflurane or ketamine was administered. **g**, Calcium activity of CANE<sub>ISO</sub>-GCaMP6m-captured CeA<sub>GA</sub> neurons tracked across isoflurane and ketamine sessions (nine mice × one trial). Neurons are aligned by the sustained activity from isoflurane GA. **h**, Left: summary of overlap using effectiveness-corrected measurement based on **c** and **e**. Green, total number of same-cell tracked neurons across sessions (*n* = 160). Cyan, isoflurane-active neurons. Orange, ketamine-active neurons. Right: the percentage of neurons activated by both ketamine and isoflurane among all isoflurane-active neurons, calculated using four methods based on the ratios between the post- and pre-stimulus activity. Green, effective time; cyan, effective mean versus mean activity; yellow, mean activity; orange, effective mean activity.

light illumination in all three groups of animals ( $CeA_{GA}-GFP, n=7$ ;  $CeA_{GA}-ChR2, n=8$ ;  $CeA_{GA}-eArch, n=7$ ). For face von Frey tests, we recorded the average number of withdrawals out of ten trials using

von Frey filaments (0.008–1.0 g). The differences between conditions with and without light illumination were calculated (Fig. 3b; exact  $P$  values for all figures are provided in Supplementary Table 1).



Without light, all three groups of mice (CeA<sub>GA</sub>-GFP, CeA<sub>GA</sub>-ChR2 and CeA<sub>GA</sub>-eArch) had no withdrawal response to filaments from 0.008 to 0.04 g applied to the face on either side. Mice began to show various numbers of head withdrawals at 0.16 g, and by 1.0 g, all animals responded reliably in all trials. Light illumination of the right CeA in control CeA<sub>GA</sub>-GFP mice ( $n=7$ ) did not induce any statistically meaningful changes in withdrawal frequencies across the entire force range (Fig. 3b, green line, and Extended Data Fig. 5a). By contrast, in CeA<sub>GA</sub>-ChR2 mice ( $n=8$ ), ChR2 activation of right CeA<sub>GA</sub> cells significantly reduced the amount of head withdrawals for both the ipsilateral and contralateral mechanical stimulations in the 0.16–0.60 g range (Fig. 3b, blue line, and Extended Data Fig. 5a). The opposite effects were observed in the CeA<sub>GA</sub>-eArch group ( $n=7$ ). Photo-silencing of the right CeA<sub>GA</sub> rendered mice hypersensitive and responsive to innocuous filaments applied to the face, especially on the ipsilateral side (Fig. 3b, purple line, and Extended Data Fig. 5a). Similar bidirectional modulation of paw responses to electronic von Frey tests were observed: ChR2-activating CeA<sub>GA</sub> markedly reduced hind paw mechanical sensitivity (on both the ipsilateral and contralateral side), whereas eArch silencing of CeA<sub>GA</sub> significantly reduced the force needed to elicit the paw withdrawal reflex for the ipsilateral hind paw (Fig. 3c). Because the effects of eArch-mediated silencing of CeA<sub>GA</sub> were much stronger on the ipsilateral side, we expressed eArch bilaterally in CeA<sub>GA</sub> using CANE in a few mice ( $n=4$ ). Stimulating the face of these mice with the 0.04 g filament normally failed to elicit any responses without photo-silencing; however, bilateral photo-silencing of CeA<sub>GA</sub> elicited withdrawal and even defensive responses to this normally

below-detection threshold filament in all four mice (Supplementary Video 3).

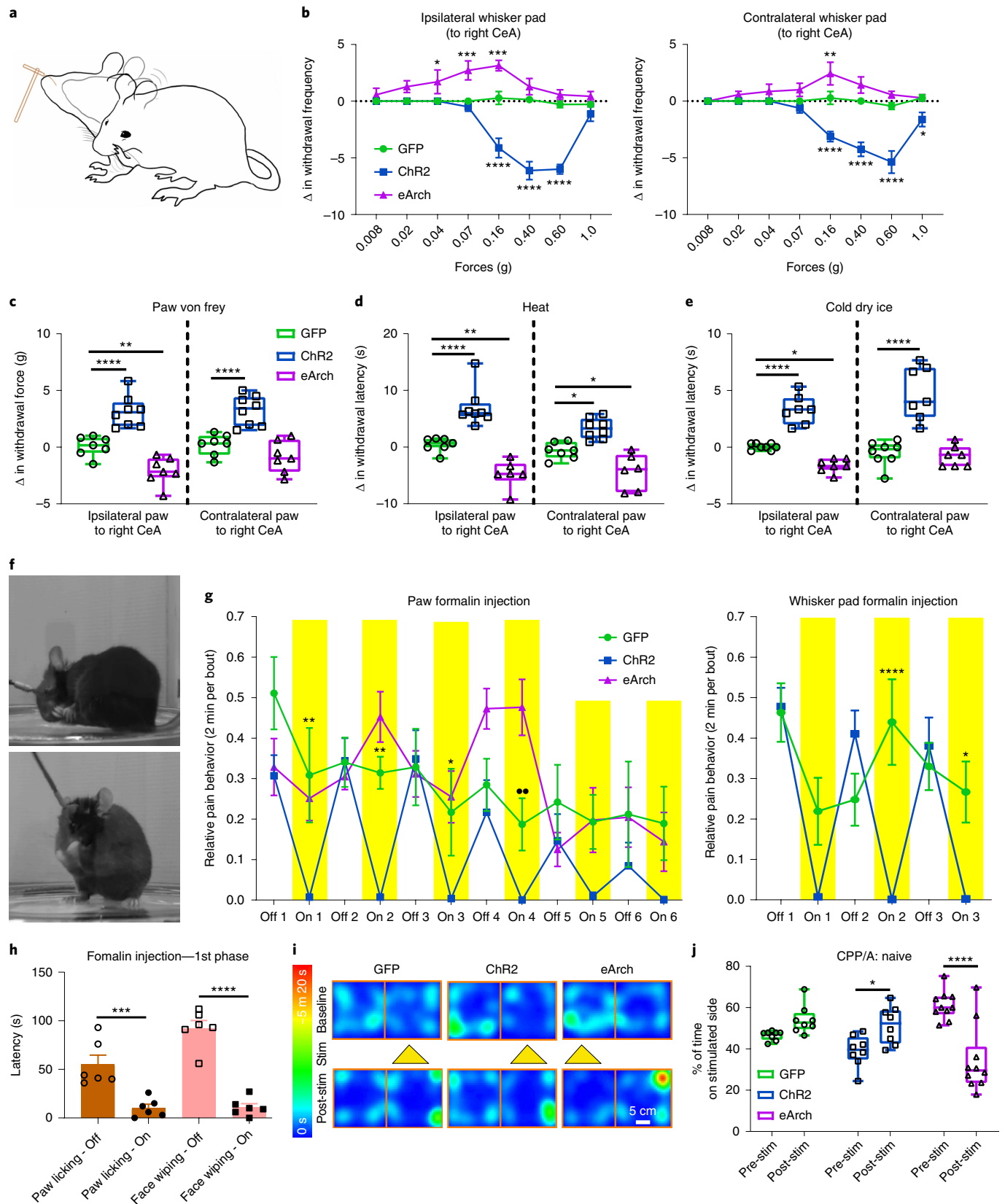
We next performed the Hargreaves heat and cold dry ice tests (Fig. 3d,e). Light illumination in the control CeA<sub>GA</sub>-GFP group did not alter animals' reflexive withdrawal behaviors in responses to heat or dry ice. Notably, photo-activation or photo-silencing of CeA<sub>GA</sub> neurons during exposure to heat and dry ice significantly increased or decreased, respectively, the withdrawal latency compared to no-light conditions or to the control groups (Fig. 3d,e, with the ipsilateral side having stronger effects). Taken together, these experiments showed that activation and silencing of CeA<sub>GA</sub> neurons can bidirectionally and potently modulate nociceptive reflex responses in naïve mice across multiple somatosensory modalities.

**Optogenetic activation or silencing of CeA<sub>GA</sub> neurons bidirectionally and potently regulated pain-elicited self-caring behaviors.** Besides reflexive defensive behaviors, more sustained pain also invokes self-caring responses such as licking and wiping, and these behaviors are thought to be indicative of pain perception. A recent study showed that there are separate neural circuits for mediating reflexive versus self-caring/recuperative behaviors<sup>21</sup>. We injected formalin into either the hind paw or the whisker pad in CeA<sub>GA</sub>-GFP (control), CeA<sub>GA</sub>-ChR2 and CeA<sub>GA</sub>-eArch mice and tested mice with or without light illumination of the CeA. Formalin caused a biphasic response: the first phase of acute pain that usually lasts a few minutes and the second phase of inflammatory pain that starts around ~20 min after formalin injection and lasts 10–15 min<sup>22,23</sup>. Mice exhibit intense licking of the hind paw or wiping of the whisker

**Fig. 3 | Activation or inhibition of CeA<sub>GA</sub> neurons bidirectionally modulated pain-related behaviors in naïve mice and acute pain models. a**, Schematic of the responses to von Frey filaments applied to the whisker pad, including head withdrawal and face wiping. **b**, Quantification of changes in the withdrawal frequency to eight different von Frey filaments in the contralateral and ipsilateral whisker pad (to the right CeA) induced by optogenetic manipulation of CeA<sub>GA</sub> neurons. Ipsilateral, control,  $n=7$  animals ( $0 \pm 0$  (0.008 g),  $0 \pm 0$  (0.02 g),  $0 \pm 0$  (0.04 g),  $0 \pm 0$  (0.07 g),  $0.29 \pm 0.57$  (0.16 g),  $0.14 \pm 0.26$  (0.40 g),  $-0.29 \pm 0.29$  (0.60 g),  $-0.29 \pm 0.18$  (1.0 g)); ChR2,  $n=8$  animals ( $0 \pm 0$  (0.008 g),  $0 \pm 0$  (0.02 g),  $0 \pm 0$  (0.04 g),  $-0.5 \pm 0.38$  (0.07 g),  $-4.13 \pm 0.85$  (0.16 g),  $-6.13 \pm 0.79$  (0.40 g),  $-6.0 \pm 0.42$  (0.60 g),  $-1.13 \pm 0.64$  (1.0 g)); and eArch,  $n=7$  animals ( $0.57 \pm 0.57$  (0.008 g),  $1.29 \pm 0.52$  (0.02 g),  $1.71 \pm 1.04$  (0.04 g),  $2.71 \pm 0.84$  (0.07 g),  $3.14 \pm 0.46$  (0.16 g),  $1.29 \pm 0.7$  (0.40 g),  $0.57 \pm 0.43$  (0.60 g),  $0.43 \pm 0.43$  (1.0 g)); two-way ANOVA; \*\*\*\* $P < 0.0001$ , \*\*\* $P < 0.001$  and \* $P < 0.05$ . Contralateral, control,  $n=7$  animals ( $0 \pm 0$  (0.008 g),  $0 \pm 0$  (0.02 g),  $0 \pm 0$  (0.04 g),  $0 \pm 0$  (0.07 g),  $0.29 \pm 0.57$  (0.16 g),  $0 \pm 0.22$  (0.40 g),  $-0.43 \pm 0.30$  (0.60 g),  $0.29 \pm 0.29$  (1.0 g)); ChR2,  $n=8$  animals ( $0 \pm 0$  (0.008 g),  $0 \pm 0$  (0.02 g),  $0 \pm 0$  (0.04 g),  $-0.63 \pm 0.42$  (0.07 g),  $-3.13 \pm 0.44$  (0.16 g),  $-4.25 \pm 0.62$  (0.40 g),  $-5.38 \pm 0.98$  (0.60 g),  $-1.63 \pm 0.63$  (1.0 g)); and eArch,  $n=7$  animals ( $0 \pm 0$  (0.008 g),  $0.57 \pm 0.30$  (0.02 g),  $0.86 \pm 0.63$  (0.04 g),  $1.0 \pm 0.58$  (0.07 g),  $2.43 \pm 1.0$  (0.16 g),  $1.43 \pm 0.72$  (0.40 g),  $0.57 \pm 0.30$  (0.60 g),  $0.29 \pm 0.29$  (1.0 g)); two-way ANOVA; \*\*\*\* $P < 0.0001$ , \*\* $P < 0.01$  and \* $P < 0.05$ ;  $F_{14,152} = 11.40$  (ipsilateral),  $F_{14,152} = 8.680$  (contralateral)). **c**, Optogenetic manipulation of CeA<sub>GA</sub>-induced changes in the withdrawal threshold in response to electronic von Frey applied to the paw (control,  $n=7$  animals ( $0.07 \pm 0.33$  g (ipsilateral),  $0.21 \pm 0.35$  g (contralateral)); ChR2,  $n=8$  animals ( $3.12 \pm 0.49$  g (ipsilateral),  $3.23 \pm 0.47$  g (contralateral)); and eArch,  $n=7$  animals ( $-2.09 \pm 0.46$  g (ipsilateral),  $-0.86 \pm 0.53$  g (contralateral)); two-way ANOVA; \*\*\*\* $P < 0.0001$ , \*\* $P < 0.01$ ;  $F_{2,38} = 49.51$ ). Data are mean  $\pm$  s.e.m. **d,e**, Quantification of the optogenetics-induced change in withdrawal latency ( $t_2 - t_1$ ) for Hargreaves heat (control,  $n=7$  animals ( $0.42 \pm 0.47$  s (ipsilateral),  $-0.67 \pm 0.54$  s (contralateral)); ChR2,  $n=8$  animals ( $7.0 \pm 1.19$  s (ipsilateral),  $3.28 \pm 0.64$  s (contralateral)); and eArch,  $n=6$  animals ( $-4.76 \pm 1.02$  s (ipsilateral),  $-4.33 \pm 1.29$  s (contralateral)); two-way ANOVA; \*\*\*\* $P < 0.0001$ , \*\* $P < 0.01$  and \* $P < 0.05$ ;  $F_{2,36} = 57.56$ ; and cold dry ice test (control,  $n=8$  animals ( $0.04 \pm 0.10$  s (ipsilateral),  $-0.51 \pm 0.38$  s (contralateral)); ChR2,  $n=7$  animals ( $3.29 \pm 0.48$  s (ipsilateral),  $4.76 \pm 0.88$  s (contralateral)); and eArch,  $n=7$  animals ( $-1.62 \pm 0.22$  s (ipsilateral),  $-0.81 \pm 0.35$  s (contralateral)); two-way ANOVA; \*\*\*\* $P < 0.0001$ , \* $P < 0.05$ ;  $F_{2,38} = 71.37$ ). Data are mean  $\pm$  s.e.m. **f**, Example images of coping behaviors, such as licking hind paw (top) or wiping whisker pad (bottom), to separate injections of formalin on different days. **g**, Quantification of self-caring behaviors (total licking duration (s)) per 2-min bins with off and on light stimulation. Hind paw formalin injection, control,  $n=8$  animals ( $0.51 \pm 0.09$  (off1),  $0.31 \pm 0.12$  (on1),  $0.34 \pm 0.06$  (off2),  $0.31 \pm 0.04$  (on2),  $0.33 \pm 0.09$  (off3),  $0.22 \pm 0.11$  (on3),  $0.28 \pm 0.06$  (off4),  $0.19 \pm 0.06$  (on4),  $0.24 \pm 0.09$  (off5),  $0.19 \pm 0.07$  (on5),  $0.21 \pm 0.13$  (off6),  $0.19 \pm 0.09$  (on6)); ChR2,  $n=9$  animals ( $0.31 \pm 0.05$  (off1),  $0.01 \pm 0.01$  (on1),  $0.34 \pm 0.06$  (off2),  $0.01 \pm 0$  (on2),  $0.35 \pm 0.07$  (off3),  $0 \pm 0$  (on3),  $0.22 \pm 0.08$  (off4),  $0 \pm 0$  (on4),  $0.15 \pm 0.07$  (off5),  $0.01 \pm 0.01$  (on5),  $0.08 \pm 0.06$  (off6),  $0 \pm 0$  (on6)); and eArch,  $n=7$  animals ( $0.33 \pm 0.07$  (off1),  $0.25 \pm 0.05$  (on1),  $0.30 \pm 0.03$  (off2),  $0.45 \pm 0.06$  (on2),  $0.31 \pm 0.06$  (off3),  $0.25 \pm 0.06$  (on3),  $0.47 \pm 0.05$  (off4),  $0.48 \pm 0.07$  (on4),  $0.13 \pm 0.04$  (off5),  $0.20 \pm 0.08$  (on5),  $0.20 \pm 0.07$  (off6),  $0.14 \pm 0.07$  (on6)); two-way repeated-measures ANOVA; \*\* $P < 0.01$  and \* $P < 0.05$ ;  $F_{5,75} = 4.81$ ; whisker pad formalin injection, control,  $n=7$  animals ( $0.46 \pm 0.07$  (off1),  $0.22 \pm 0.08$  (on1),  $0.25 \pm 0.06$  (off2),  $0.44 \pm 0.11$  (on2),  $0.33 \pm 0.06$  (off3),  $0.27 \pm 0.08$  (on3)); ChR2,  $n=9$  animals ( $0.48 \pm 0.05$  (off1),  $0.01 \pm 0.01$  (on1),  $0.41 \pm 0.06$  (off2),  $0 \pm 0$  (on2),  $0.38 \pm 0.07$  (off3),  $0 \pm 0$  (on3)); two-way repeated-measures ANOVA; \*\*\*\* $P < 0.0001$  and \* $P < 0.05$ ;  $F_{5,70} = 8.825$ ). Data are mean  $\pm$  s.e.m. **h**, Quantification of total wiping and licking behaviors during the first phase after formalin injection comparing off and on stimulation (2-min bins with off and on light stimulation, total 6 min of stimulation) (ChR2,  $n=6$  animals ( $55.00 \pm 21.56$  s (licking-off),  $10.33 \pm 8.65$  s (licking-on),  $92.33 \pm 17.84$  s (wiping-off),  $11.00 \pm 8.33$  s (wiping-on)); one-way ANOVA; \*\*\* $P < 0.001$  and \*\*\*\* $P < 0.0001$ ;  $F_{3,20} = 33.55$ ). **i**, Example heat map of CPP/CPA experiment. **j**, Quantification of the percent of time (%) naïve mice spent on the stimulated side (control,  $n=8$  animals ( $46.52 \pm 0.80$  (pre),  $54.16 \pm 2.45$  (post)); ChR2,  $n=8$  animals ( $39.05 \pm 2.70$  (pre),  $51.54 \pm 3.20$  (post)); and eArch,  $n=10$  animals ( $61.16 \pm 2.17$  (pre),  $34.39 \pm 5.11$  (post)); two-way repeated-measures ANOVA; \*\*\*\* $P < 0.0001$  and \* $P < 0.05$ ;  $F_{2,23} = 29.66$ ). Data are mean  $\pm$  s.e.m.

ker pad during the second phase (Fig. 3f,g)<sup>22,23</sup>. At the start of the second phase, we first video-recorded animals' behavior for 2 min and then illuminated the CeA<sub>GA</sub> neurons every 2 min for three to six times. Remarkably, ChR2 activation of CeA<sub>GA</sub> neurons (unilaterally)

completely abolished paw-licking or face-wiping behavior regardless of whether the right or left paw or whisker pad was injected with formalin, as compared to the persistent self-recuperating behaviors of CeA<sub>GA</sub>-GFP mice that were unaffected by light (Fig. 3g). As soon



as CeA<sub>GA</sub> was activated, the mice stopped licking (Supplementary Video 4 and Fig. 3g, left) or wiping (Supplementary Video 5 and Fig. 3g, right) and simply walked around the cage. In the initial 2 min after light stimulation, control CeA<sub>GA</sub>-GFP mice also decreased face-wiping time (Fig. 3g, right). This might be due to either the initial distraction of the light or other unknown effects of light on CeA neurons. ChR2 activation of CeA<sub>GA</sub> neurons also drastically reduced licking and wiping behavior in the first phase of acute pain induced by formalin injection ( $n=6$ , Fig. 3h). Note that activating CeA<sub>GA</sub> neurons did not have any effect on mating behaviors as measured by the number of ultrasonic vocalization syllables and the duration of anogenital sniffing/mounting (Extended Data Fig. 5c,d). Thus, the ceasing of the self-caring behaviors upon ChR2 activation of CeA<sub>GA</sub> neurons is unlikely due to the suppression of general motivation.

Formalin-induced self-caring behaviors gradually subsided after ~10 min in the second phase, because inflammation responses decreased over time, but the affected area was likely still sensitive. We asked what happened if we optogenetically silenced CeA<sub>GA</sub> neurons during this period in the hind paw formalin test. Initially in the beginning of the second phase, animals with eArch silencing of CeA<sub>GA</sub> neurons behaved similarly to control CeA<sub>GA</sub>-GFP mice, perhaps because mice already licked constantly at early stages (Fig. 3g, On 1 and 2); and after several bouts of inhibiting CeA<sub>GA</sub> at early stages, mice started licking their paws even when the light was off (Fig. 3g, Off 4). Interestingly, at later stages (>8 min into the second phase), when mice exhibited low levels of paw licking, photo-silencing of CeA<sub>GA</sub>-eArch mice immediately re-elicited robust licking toward the inflamed paw (Supplementary Video 6 and Fig. 3g). Hence, when CeA<sub>GA</sub> neurons were silenced, animals appeared to perceive the subsided injury as becoming intense or painful again. Taken together, these experiments showed that activation and silencing of CeA<sub>GA</sub> neurons can bidirectionally and potentially regulate pain-elicited intentional self-caring behaviors.

**Partial lateralization of CeA<sub>GA</sub> functions.** Most of the experiments described above were performed by manipulating either the right or both the right and left CeA<sub>GA</sub> neurons. We next tested whether there could be a lateralization of CeA<sub>GA</sub> functions by activating only the left CeA<sub>GA</sub> cells. In CeA<sub>GA</sub>-ChR2<sub>LEFT</sub> mice ( $n=6$ ), ChR2 activation of the left CeA<sub>GA</sub> reduced the amount of paw withdrawals for both the ipsilateral and contralateral paw in the von Frey test (in the 1.0–2.0-g force range, Extended Data Fig. 6a). Surprisingly, in the face von Frey test, activation of left CeA<sub>GA</sub> neurons did not produce any observable changes in head withdrawal responses (Extended Data Fig. 6b). On the other hand, for cold and heat, as well as paw-formalin and face-formalin tests ( $n=7$  CeA<sub>GA</sub>-ChR2<sub>LEFT</sub> mice), ChR2 activation of left CeA<sub>GA</sub> cells increased the withdrawal latencies (Extended Data Fig. 6c) and drastically reduced licking and wiping behaviors in all tests (Extended Data Fig. 6d). Thus, except for the partial lateralization of the role for suppressing facial

mechanical sensitivity to the right side, activation of left CeA<sub>GA</sub> neurons produced similar results as those of the right CeA<sub>GA</sub>.

### In vivo imaging of CeA<sub>GA</sub> neuron activity during sensory tests.

The findings that optogenetic silencing of CeA<sub>GA</sub> neurons rendered CeA<sub>GA</sub>-eArch mice hypersensitive to mechanical, heat and cold stimuli, and exacerbated pain-elicited caring behaviors raised the possibility that the basal level (ongoing) activity of CeA<sub>GA</sub> neurons function to prevent behavioral hypersensitivity. We next asked whether the spontaneous activity of CeA<sub>GA</sub> neurons would change in response to noxious stimuli in awake behaving mice. We performed in vivo calcium imaging of CANE<sub>ISO</sub>-GCaMP6m captured CeA<sub>GA</sub> neurons while performing heat, cold or von Frey stimuli in awake behaving mice (Fig. 4b). To avoid any potential photodamage caused by prolonged imaging, different sensory tests were performed on different days with at least a 1-d interval between the tests. The animals' behaviors were tracked using video-recordings (Fig. 4a,c and Methods).

In vivo calcium imaging revealed that, as a population, there were no apparent time-locked changes in CeA<sub>GA</sub> neuron activity regarding the onset of the heat, cold or von Frey stimuli (Extended Data Fig. 7) or to the onset of withdrawal reflex responses or the withdrawal of the stimuli by the experimenter (Fig. 4d,f,h,j). The ongoing activity of individual CeA<sub>GA</sub> neurons was distributed across the trial period, and the averaged population activity was flat (average is shown on top of each heat map), suggesting that CeA<sub>GA</sub> neuron activity was uncorrelated and unresponsive to acutely applied sensory stimuli.

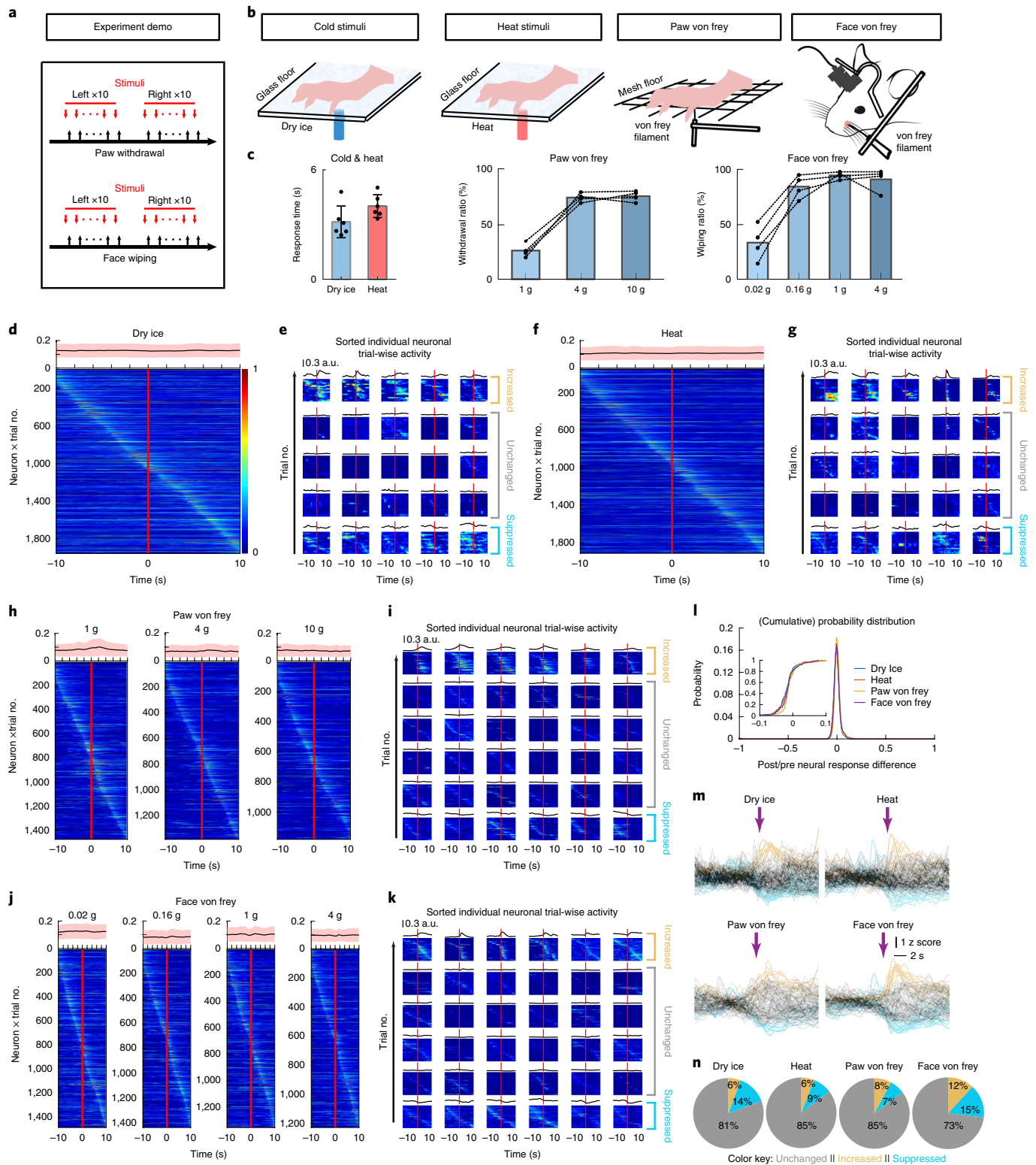
We also analyzed the activity of individual CeA<sub>GA</sub> neurons. In all tests, neurons could be classified into three groups: (1) activity increased, (2) activity unchanged (nonresponsive to stimuli) and (3) activity suppressed (see heat maps of many example cells in Fig. 4e,g,i,k, averaged traces shown in Fig. 4m and percentages of the three types of neurons in each test shown in Fig. 4n). For each neuron, we also computed the difference between post- and pre-stimulus calcium signal intensity and plotted the distributions across four sensory tests (Fig. 4l). In all cases, most imaged neurons did not alter their activity upon noxious stimuli applications in agreement with the averaged population activity data. These results suggest that the ongoing activity of CeA<sub>GA</sub> neurons might largely reflect the animal's internal state rather than the immediate experience of noxious stimuli. Consistent with the imaging results, we found that CANE-GFP-captured CeA<sub>GA</sub> neurons had minimal overlap with formalin-pain-activated Fos<sup>+</sup> CeA nociceptive neurons (Extended Data Fig. 8a).

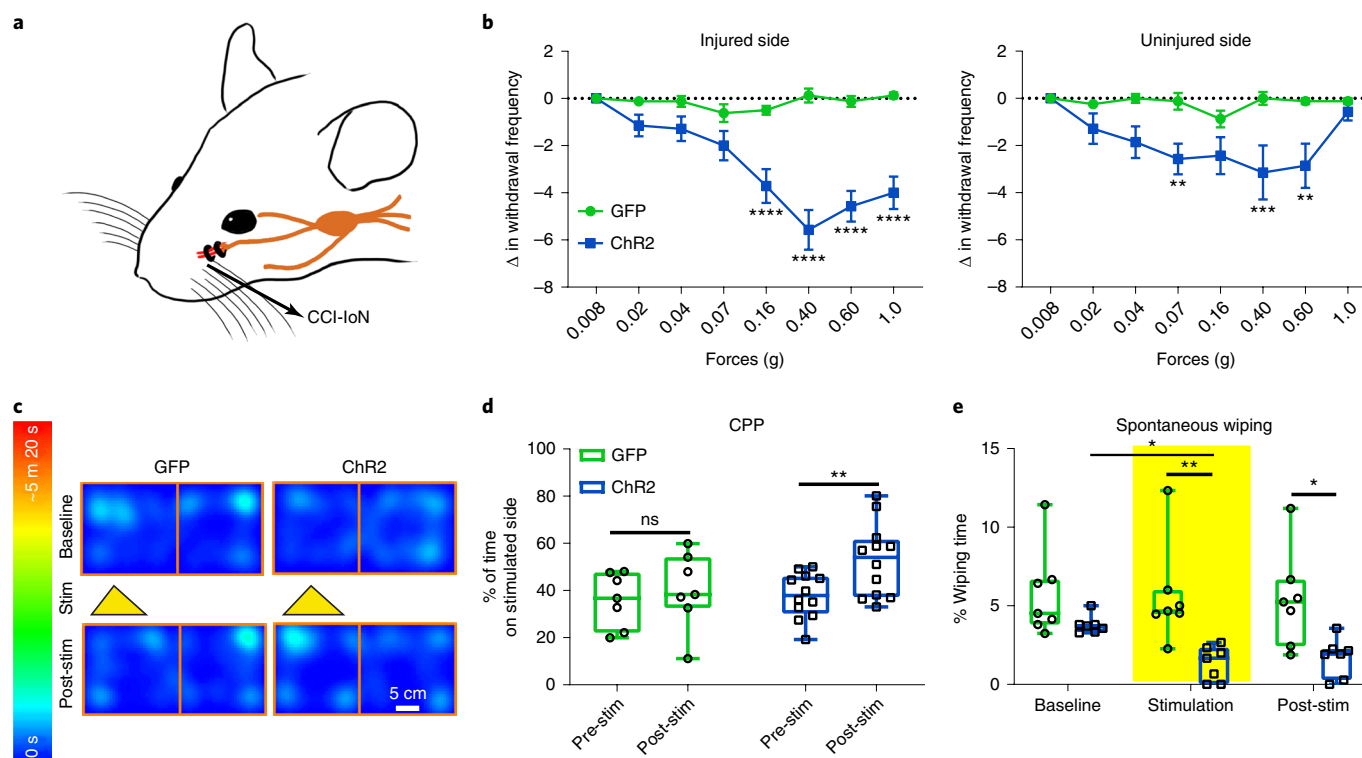
**Silencing CeA<sub>GA</sub> neurons is aversive in the absence of noxious stimuli.** An essence of the pain experience is aversion, or the perceived negative effect. If the observed ongoing CeA<sub>GA</sub> activity indeed functions to prevent abnormal hypersensitivity to non-noxious stim-

**Fig. 4 | In vivo calcium imaging of CeA<sub>GA</sub> activities in sensory tests.** **a**, Scheme of nociceptive stimuli on mice hind paws and facial pads. Red arrows, onset of stimuli. Black arrows, onset of withdrawal reflex responses. **b**, Diagram showing calcium imaging of CeA<sub>GA</sub> neurons during cold, heat and graded von Frey stimuli applied to the hind paws in freely moving mice or von Frey stimuli applied to the whisker pads in head-fixed mice. **c**, Left: paw withdrawal latencies in response to dry ice ( $3.16 \pm 0.36$  s) and heat stimuli ( $4.02 \pm 0.26$  s) ( $n=6$  animals). Middle: the percentage (%) of paw withdrawal in response to each filament of von Frey stimuli ( $n=4$  animals ( $26.25 \pm 3.17\%$  (1 g),  $75.00 \pm 2.08\%$  (4 g),  $76.25 \pm 2.43\%$  (10 g)). Right: the percentage of face wiping in response to each filament of von Frey stimuli ( $n=4$  animals,  $35.00 \pm 8.42\%$  (0.02 g),  $88.75 \pm 5.54\%$  (0.16 g),  $99.50 \pm 1.71\%$  (1.0 g),  $95.75 \pm 5.31\%$  (4.0 g)). Data are mean  $\pm$  s.e.m. **d,f,h,j**, Neuronal activity patterns during cold stimuli (**d**), heat stimuli (**f**), von Frey stimuli to paws (**h**) and von Frey stimuli to facial pads (**j**) sorted by neurons peak responses timing (from  $-10$  to  $+10$  s, 0 is the onset of response; for those trials without response in the von Frey stimuli, 0 is the withdrawal of von Frey filament). Top of each heat map, averaged population activity. Thick lines indicate mean, and shaded areas indicate s.e.m. **e,g,i,k**, Three patterns of representative individual neuron responses plotted for all the trials to **e**, **g**, **i** and **k**, sorted by neurons peak responses timing (from  $-10$  to  $+10$  s). Mean response of each neuron was plotted on the top of each corresponding heat map. **l**, Probability distribution (inset: cumulative probability distribution) of neural response differences between post- and pre-response to calcium signal intensity during the four sensory tests. **m**, Averaged calcium traces of individual neuron responses to noxious stimuli. Individual trial response was plotted in black (unchanged neurons), blue (suppressed neurons) and yellow (activated neurons). **n**, Percentage of three response types of CeA<sub>GA</sub> neurons during four sensory tests.

uli, silencing these neurons would lead to allodynia in an otherwise innocuous environment and therefore could be aversive for mice. To test this, we subjected  $CeA_{GA}$ -GFP,  $CeA_{GA}$ -ChR2 and  $CeA_{GA}$ -eArch mice to Conditioned Place Preference (CPP) and Conditioned Place Aversion (CPA) tests over a period of 6 d. On day 1, animals were left to freely explore a two-chamber box. On days 2 and 4,  $CeA_{GA}$ -GFP and  $CeA_{GA}$ -ChR2 animals received photo-illumination of the  $CeA_{GA}$  when they were in the less-preferred chamber and received no stim-

ulation in the preferred chamber on days 3 and 5.  $CeA_{GA}$ -eArch animals received photo-illumination in the preferred chamber. On day 6, animals were re-tested for their preference. Both  $CeA_{GA}$ -GFP and  $CeA_{GA}$ -ChR2 mice moderately preferred the photo-illuminated side; however, the preference was only statistically significant for  $CeA_{GA}$ -ChR2 mice (Fig. 3i,j). Notably, in  $CeA_{GA}$ -eArch animals, silencing of  $CeA_{GA}$  dramatically changed their preference, leading to significant avoidance of the chamber where they had experienced





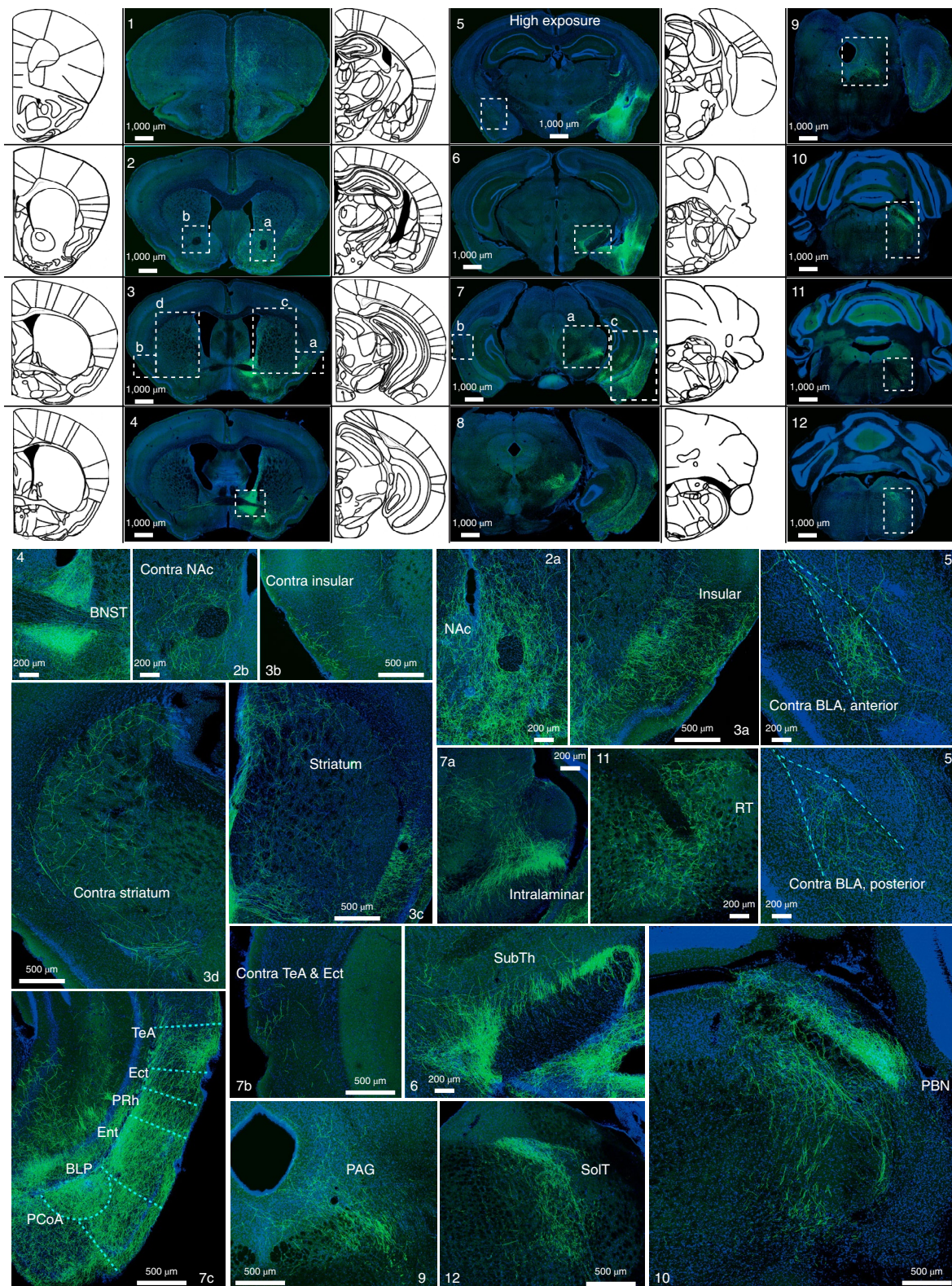
**Fig. 5 | Activation of  $CeA_{GA}$  neurons strongly reduced nociception-related behaviors in the CCI model and drove CPP.** **a**, Schematic of the site of CCI of the infraorbital nerve. **b**, Quantification of activating  $CeA_{GA}$ -induced changes in withdrawal frequency to eight different von Frey filaments in the injured and non-injured side of the whisker pad after IoN-CCI. Injured side, control,  $n = 8$  animals ( $0 \pm 0$  (0.008 g),  $-0.13 \pm 0.13$  (0.02 g),  $-0.13 \pm 0.23$  (0.04 g),  $-0.63 \pm 0.38$  (0.07 g),  $-0.50 \pm 0.19$  (0.16 g),  $0.13 \pm 0.30$  (0.40 g),  $-0.13 \pm 0.23$  (0.60 g),  $0.13 \pm 0.13$  (1.0 g)); ChR2,  $n = 7$  animals ( $0 \pm 0$  (0.008 g),  $-1.14 \pm 0.46$  (0.02 g),  $-1.29 \pm 0.52$  (0.04 g),  $-2.00 \pm 0.62$  (0.07 g),  $-3.71 \pm 0.71$  (0.16 g),  $-5.57 \pm 0.84$  (0.40 g),  $-4.57 \pm 0.65$  (0.60 g),  $-4.00 \pm 0.69$  (1.0 g)); two-way ANOVA; \*\*\*\* $P < 0.0001$ ;  $F_{7,104} = 10.74$ . Uninjured side, control,  $n = 8$  animals ( $0 \pm 0$  (0.008 g),  $-0.25 \pm 0.16$  (0.02 g),  $0 \pm 0.19$  (0.04 g),  $-0.13 \pm 0.35$  (0.07 g),  $-0.88 \pm 0.35$  (0.16 g),  $0 \pm 0.27$  (0.40 g),  $-0.13 \pm 0.13$  (0.60 g),  $-0.13 \pm 0.13$  (1.0 g)); ChR2,  $n = 7$  animals ( $0 \pm 0$  (0.008 g),  $-1.29 \pm 0.64$  (0.02 g),  $-1.86 \pm 0.67$  (0.04 g),  $-2.57 \pm 0.65$  (0.07 g),  $-2.43 \pm 0.78$  (0.16 g),  $-3.14 \pm 1.14$  (0.40 g),  $-2.86 \pm 0.94$  (0.60 g),  $-0.57 \pm 0.37$  (1.0 g)); two-way ANOVA; \*\* $P < 0.01$  (0.07 g), \*\*\* $P < 0.001$  (0.40 g), \*\* $P < 0.01$  (0.60 g);  $F_{7,104} = 2.393$ ). Data are mean  $\pm$  s.e.m. **c**, Example heat map of CPP/CPA experiment. Control and ChR2 mice received stimulation on non-preferred side. **d**, Quantification of the percent of time spent on the stimulated side after CCI (control,  $n = 7$  animals ( $35.92 \pm 4.38$  (pre),  $40.17 \pm 6.09$  (post)) and ChR2,  $n = 12$  animals ( $37.87 \pm 2.76$  (pre),  $52.74 \pm 4.48$  (post)); two-way ANOVA; \*\* $P < 0.01$  and  $P = 0.80$  (NS);  $F_{1,17} = 7.185$ ). Data are mean  $\pm$  s.e.m. **e**, Quantification of percent of time-eliciting spontaneous wiping after CCI before, during and after light stimulation (control,  $n = 7$  and ChR2,  $n = 7$  animals; 7 min baseline of no light ( $5.75 \pm 1.07$  (control) and  $3.79 \pm 0.22$  (ChR2)), followed by 5 min of light stimulation ( $5.61 \pm 1.20$  (control) and  $1.33 \pm 0.42$  (ChR2)) and another 7 min post-stimulation ( $5.37 \pm 1.16$  (control) and  $1.73 \pm 0.46$  (ChR2)); two-way repeated-measures ANOVA; \*\* $P < 0.01$  and \* $P < 0.05$ ;  $F_{1,12} = 11.98$ ). Data are mean  $\pm$  s.e.m.

photo-silencing (Fig. 3i,j). Thus, silencing  $CeA_{GA}$  neurons induced a strong place aversion in mice in the absence of noxious stimuli.

**Activation of  $CeA_{GA}$  neurons strongly reduced nociception-related behaviors in a chronic neuropathic pain model.** The next key question was whether activating  $CeA_{GA}$  neurons can suppress mechanical hypersensitivity in chronic neuropathic pain conditions. We subjected  $CeA_{GA}$ -GFP and  $CeA_{GA}$ -ChR2 mice to a chronic orofacial neuropathic pain model in which the infraorbital nerve (IoN) was ligated on the right side of the face, referred to as chronic constriction injury (CCI, Fig. 5a). This injury caused persistent sensitization of the whisker pad on the IoN-ligated side to non-noxious tactile stimuli<sup>24</sup>. In the face von Frey test, without photo-stimulation, CCI-IoN mice started to show withdrawal responses to the normally innocuous 0.02-g force on both sides (Fig. 5b, the blue curve deviates from the control green curve at 0.02 g in both sides, indicating that activating  $CeA_{GA}$  reduced the hypersensitive withdrawal responses to the innocuous filaments; see also Extended Data Fig. 5b). This is consistent with the known mechanical hypersensitivity, or allodynia, induced by neuropathic pain, including the so-called mirror pain on the uninjured side (Fig. 5b, right)<sup>25,26</sup>. Remarkably,

unilateral ChR2 activation of  $CeA_{GA}$  neurons (right,  $CeA_{GA}$ ) dramatically reduced the withdrawal responses on the injured side (right side), as many animals simply showed no responses at all, even to 1.0 g stimulation (Fig. 5b, left blue line, and Supplementary Video 7), whereas illuminating control  $CeA_{GA}$ -GFP animals did not alter their sensitivity to the entire range of filaments (Fig. 5b, green line, and Supplementary Video 8). Note that, in the naïve condition and for the uninjured side, a 1.0 g von Frey stimulus applied to the face elicited consistent withdrawal reflexes even with ChR2 activation of  $CeA_{GA}$  (Fig. 3b). By contrast, under CCI-IoN, activation of  $CeA_{GA}$  revealed that the injured side was impaired at responding to 1.0 g (that is, hyposensitive at the periphery), thereby suggesting that mechanical hypersensitivity in neuropathic pain conditions mostly results from abnormal central processing.

We also performed a CPP test in CCI-IoN animals. Photo-activation of  $CeA_{GA}$  neurons in  $CeA_{GA}$ -ChR2 mice but not in control  $CeA_{GA}$ -GFP mice produced a place preference memory for the light-activated chamber, presumably due to pain relief received in that chamber (Fig. 5c,d). Furthermore, CCI-IoN animals exhibited spontaneous asymmetric face wiping of the injured side, an indicator of their perceiving spontaneous pain. ChR2 activation of



**Fig. 6 | Whole-brain mapping of axonal projections from CeA<sub>GA</sub> neurons.** Top: Coronal schematic next to example coronal slices. Boxes indicate the location of high-magnification zoomed-in view of axonal projections. Bottom: in sequential order: 1, cortex; 2a, nucleus accumbens (NAc); 2b, contralateral NAc; 3a, insular, 3b, contralateral insular; 3c, striatum, 3d, contralateral striatum; 4, bed nucleus stria terminalis (BNST); 5, contralateral basal amygdala (BLA, top, anterior; bottom, posterior); 6, subthalamal nucleus (SubTh); 7a, posterior intralaminar nucleus of thalamus; 7b, contralateral temporal association cortex (TeA); 7c, TeA, ectorhinal cortex (Ect), perirhinal cortex (PRh), entorhinal cortex (Ent), posterior basal lateral amygdala (BLP), posterior cortical amygdala nucleus (PCoA); 8, posterior TeA, Ect, Ent and midbrain reticular nucleus (RR); 9, periaqueductal gray (PAG); 10, parabrachial nucleus (PBN); 11, rostral reticular formation (RT); and 12, nucleus of solitary tract (SolT) and caudal intermediate reticular formation. Repeated experiments for  $n=5$  biologically independent samples.

CeA<sub>GA</sub> neurons in CeA<sub>GA</sub>-Chr2 mice (but not photo-illumination of the CeA in CeA<sub>GA</sub>-GFP mice) significantly reduced the total wiping duration in CCI-IoN mice (Fig. 5e), and there was also a lasting effect in the post-stimulation period (Fig. 5e). Taken together, activation of the CeA<sub>GA</sub> can potentially suppress pain-related behaviors in the chronic neuropathic pain model.

**CeA<sub>GA</sub> neurons project broadly to many pain-processing centers in the brain to suppress their activity.** To further understand how CeA<sub>GA</sub> neurons exert their analgesic effects, we traced the axonal projections of CeA<sub>GA</sub> neurons in CeA<sub>GA</sub>-GFP mice. The potential downstream targets of CeA<sub>GA</sub> neurons included the prefrontal cortex (pre-limbic and cingulate), the nucleus accumbens (NAc), the dorsal medial striatum, the insular cortex (Ins), the bed nucleus of stria terminalis (BNST), the BLA, the cortical amygdaloid nucleus (PMCo, PLCo), the temporal association cortex (TeA), the entorhinal cortex (Ect), entorhinal cortex (Ent), the subthalamic and peri-subthalamic region (SubTh), the posterior intralaminar nucleus of the thalamus, the ventrolateral periaqueductal gray (PAG), the parabrachial nucleus (PBN), the reticular nucleus (RT, mostly the intermediate RT) and the nucleus of the solitary tract (SolT) (Fig. 6). Many of these regions had previously been indicated in processing sensory or emotional aspects of pain<sup>27–30</sup>. Notably, most previous studies did not find a direct projection from the CeA to the prefrontal cortex. Future studies with more precise molecular-marker-based CeA<sub>GA</sub> labeling methods will be needed to validate this connection. The contralateral side of the NAc, striatum, Ins, BLA and TeA/Ect were also innervated, albeit more sparsely compared to the ipsilateral equivalent (Fig. 6). Such bilateral projections could explain the bilateral effects with ipsilateral bias of activating CeA<sub>GA</sub> unilaterally (Fig. 3). Because the BLA is immediately adjacent to the CeA where the CeA<sub>GA</sub> cells are labeled, the long exposure time resulted in saturated fluorescent images of the CeA and BLA region (Fig. 6, (v)). A lower exposure at higher magnification showed that CeA<sub>GA</sub> axons but not BLA cell bodies were labeled (Extended Data Fig. 8b). Representative images of CeA<sub>GA</sub>-axon projections in each of the target areas from multiple different mice and the quantifications of the averaged projection densities are shown (Extended Data Fig. 9).

Furthermore, we noted that many of CeA<sub>GA</sub> neurons' axonal targets contained formalin-pain-induced Fos<sup>+</sup> neurons (white-colored nuclei in Fig. 7a,c; these areas are the same brain regions shown in Fig. 6). Considering that CeA<sub>GA</sub> neurons are GABAergic, in principle they are in an ideal position to potentially suppress the activities of these pain-activated neurons through their projections. Indeed, CeA<sub>GA</sub>-Chr2 mice that received bilateral optogenetic activation of CeA<sub>GA</sub> ( $n=3$ ) showed significantly reduced numbers of Fos<sup>+</sup> neurons in all CeA<sub>GA</sub> target regions (compare Fig. 7b,d to Fig. 7a,c, quantification in Fig. 7e). Thus, CeA<sub>GA</sub> neurons can potentially inhibit

neural activation across numerous pain-processing centers in the brain.

**Activity of CeA<sub>GA</sub> neurons is required for the analgesic effect of low-dose ketamine.** We started this study by hypothesizing that the analgesic effect of general anesthetics is separable from the GA-induced loss of consciousness, especially at low GA drug concentrations. Indeed, when we imaged the in vivo activity of CANE<sub>ISO</sub>-GCaMP6m neurons, captured with 1.5% isoflurane, we found that more neurons became sustainably activated in response to the 0.5% isoflurane (total of 106 same neurons tracked between 1.5% and 0.5% isoflurane sessions, Extended Data Fig. 10a,b). Because it is difficult to perform behavioral tests under low-dose isoflurane in the gas/induction chamber, we turned to low-dose ketamine, which is clinically known to have an analgesic effect. Previous studies showed that, at 12 mg kg<sup>-1</sup>, ketamine can reduce pain behavioral responses in mice<sup>31</sup>. We tracked the activity of 69 CANE<sub>ISO</sub>-GCaMP6m captured CeA<sub>GA</sub> neurons across three imaging sessions—1.5% isoflurane, regular-dose ketamine (100 mg kg<sup>-1</sup>) and low-dose ketamine (12 mg kg<sup>-1</sup>)—and found that most of the tracked neurons were activated in all three conditions, including low-dose ketamine (Extended Data Fig. 10c,d).

To test whether the activity of CeA<sub>GA</sub> neurons is required for the analgesic effect of low-dose ketamine, we subjected CeA<sub>GA</sub>-eArch mice ( $n=8$ ) to the capsaicin test. After injection of capsaicin (2 μg per 10 μl) into the paw, the saline (i.p.) group ( $n=5$ ) elicited robust paw licking. Low-dose ketamine significantly reduced the duration of licking ( $n=4$ ) (Fig. 7f). Notably, when CeA<sub>GA</sub> neurons were optogenetically silenced (silenced for the first and last 5 min out of the total 15 min) in the capsaicin + ketamine conditions, mice licked the paw for a similar amount of time as that in capsaicin + saline conditions, hence the analgesic effect of ketamine was abolished (Fig. 7f). This result revealed that the activity of CeA<sub>GA</sub> neurons is required for the pain-relieving effect of low-dose ketamine.

## Discussion

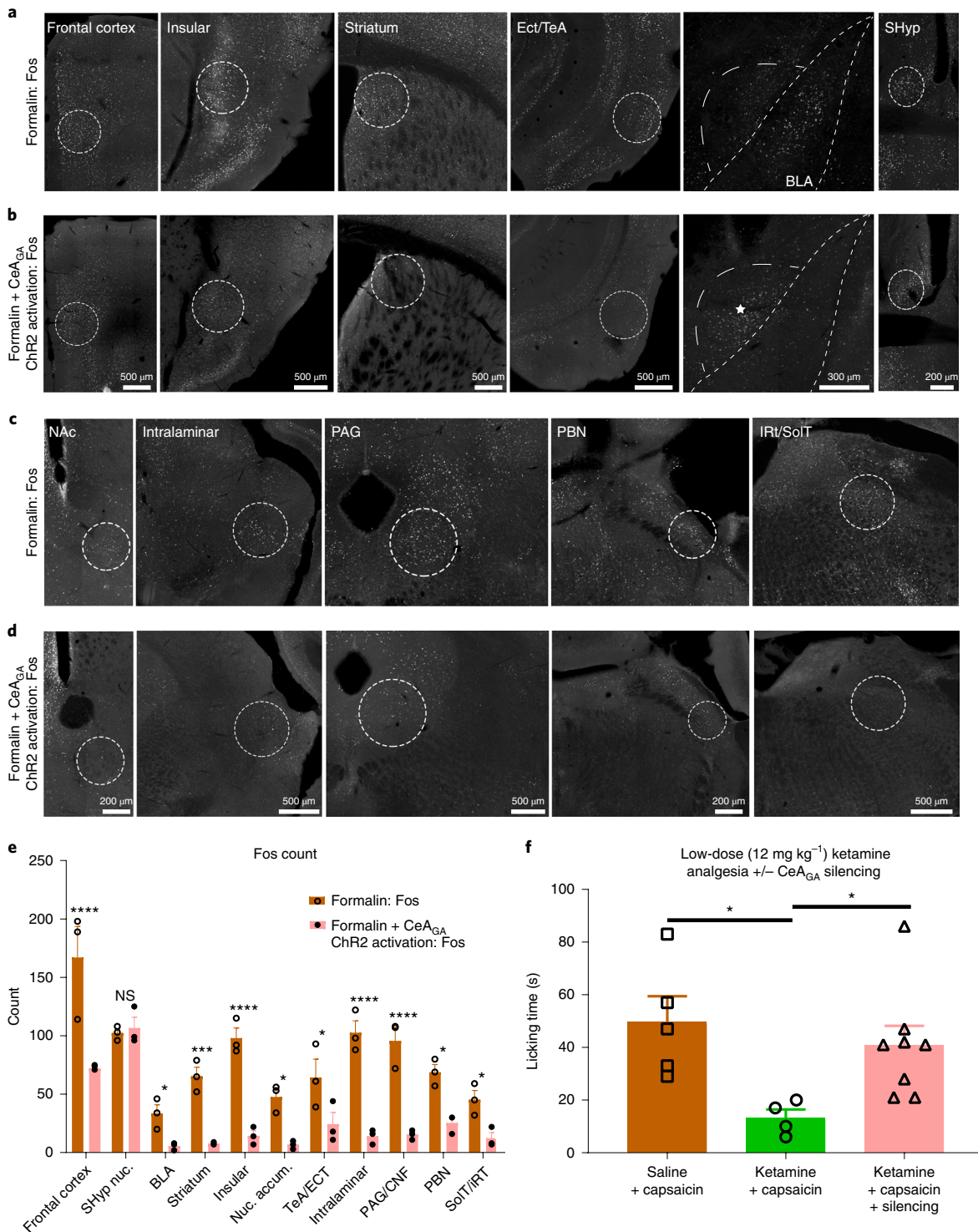
The existence of a central analgesic system was first postulated based on a seminal study published in 1946 by H.K. Beecher (a physician who served in the US Army during World War II), who showed that badly wounded soldiers, although alert and not in shock, did not report pain or a need for medication<sup>32</sup>. This finding triggered the subsequent search for the brain's internal analgesic system. Furthermore, the clinically important phenomenon called placebo analgesia also suggests the existence of a central pain suppression system<sup>33–35</sup>, but the exact circuits carrying out the placebo effect are unknown. Over the past decades, important progress was made that delineated a midbrain periaqueductal gray-brainstem-spinal descending pain modulation pathway<sup>36–38</sup>; however, whether the forebrain contains a central analgesic center and how it might

**Fig. 7 | Activation of CeA<sub>GA</sub> neurons reduced formalin-induced activity to all CeA<sub>GA</sub> target regions, and silencing CeA<sub>GA</sub> blocked the analgesic effect of low-dose ketamine. a,c**, Representative images of strong Fos<sup>+</sup> expression induced by formalin. The regions shown here are all CeA<sub>GA</sub> targets revealed in Fig. 6, including frontal cortex, insular, striatum, entorhinal (Ect), temporal association cortex (TeA), basolateral amygdala (BLA), nucleus accumbens (NAc), intralaminar, periaqueductal gray (PAG), parabrachial nucleus (PBN), intermediate reticular nucleus (iRT) and solitary tract (SolT). Note that the septohypothalamic nucleus (SHyp) does not receive projections from CeA<sub>GA</sub> neurons and serves as a negative control. **b,d**, Representative images of reduced Fos<sup>+</sup> expression with Chr2 activation of CeA<sub>GA</sub> neurons (captured with CANE under isoflurane) after formalin injection in those same brain regions as in **a** and **c**. Note that \* signifies the CeA<sub>GA</sub> cells activated under Chr2. Imaging shown in **a–d** was repeated for  $n=3$  biologically independent samples. **e**, Quantification of averaged Fos<sup>+</sup> cell count in areas that receive CeA<sub>GA</sub> neuron projections induced by formalin (**a,c**) or formalin plus Chr2 activation of CeA<sub>GA</sub> (**b,d**). Cell count represents the total number of cells from sections containing each of the regions but using only a single focal plane from each section for counting. Formalin Fos,  $n=3$  biologically independent samples; Formalin + CeA<sub>GA</sub>-Chr2 Fos,  $n=3$  biologically independent samples; two-way ANOVA; \*\*\*\* $P < 0.0001$  (FC, Ins, intralaminar, PAG), \*\*\* $P < 0.001$  (striatum), \* $P < 0.05$  (BLA, NAc, TeA/Ect, PBN and SolT,  $P > 0.999$  (NS));  $F_{1,44} = 186.8$ . **f**, Quantification of total licking time (s) in response to capsaicin injection into the paw with co-administration (i.p.) of saline or low-dose (12 mg kg<sup>-1</sup>) ketamine with or without optogenetic silencing of CeA<sub>GA</sub> neurons that were captured with CANE under isoflurane (saline + capsaicin,  $n=5$  animals (40.80 ± 24.1 s); ketamine + capsaicin,  $n=4$  animals (12.25 ± 6.94 s); ketamine + capsaicin + silencing,  $n=8$  animals (34.75 ± 12.93 s); one-way ANOVA with unpaired *t*-test, two-tailed; \* $P < 0.05$ ;  $F_{2,14} = 4.447$ ).

work remains unknown. In this study, starting with the hypothesis that GA-induced analgesia is an active process, we discovered and delineated CeA<sub>GA</sub> neurons as a key node in the central nervous system that are activated by GA, function to potently suppress pain responses in both acute and chronic conditions, project to numerous pain-processing centers and mediate the analgesic effects of general anesthetics (that is, independent of their sedative effect).

Interestingly, the CeA has previously been implicated as a critical structure for both stress- and placebo-induced analgesia<sup>34,39,40</sup>, and lesions of the CeA abolish such analgesia in rats<sup>41</sup>. However, owing

to the multi-functional nature of the CeA, which includes regulating innate and learned fear, pain (both pro-pain and anti-pain), and appetitive/feeding-related behaviors<sup>9,14,42–44</sup>, as well as its molecular heterogeneity<sup>13</sup>, it was unknown what subsets of CeA neurons are involved in analgesia. It is also unknown whether stress and placebo employ different or same CeA neurons for analgesia. Note that stress is a double-edged sword—that is, stress can either enhance or reduce pain depending on different contexts<sup>39,45</sup>. In our study, most CeA<sub>GA</sub> neurons were suppressed by restraint stress (Extended Data Fig. 3), suggesting that CeA<sub>GA</sub> might not be involved in



stress-induced analgesia (SIA). Furthermore, activating CeA<sub>GA</sub> neurons had no effect on fear- or anxiety-like behaviors (Extended Data Fig. 4), whereas SIA is often induced by fear and is considered as part of the fight-or-flight responses<sup>39,45</sup>. Hence, it is possible that CeA neurons involved in fear responses are more likely to be involved in SIA. Along this line, *Sst*-expressing CeA neurons, which are non-overlapping with CeA<sub>GA</sub> neurons revealed here and are known to mediate the fear-induced freezing responses, were shown in a recent study to attenuate pain responses<sup>46</sup>. However, a small number of CeA<sub>GA</sub> neurons were activated by stress (Extended Data Fig. 3). Thus, we cannot rule out the possibility that strong stressors, such as acute life-threatening conditions, might activate more CeA<sub>GA</sub> neurons to produce analgesia. It will also be interesting to test, in the future, whether CeA<sub>GA</sub> is involved in placebo analgesia.

Both our molecular marker analyses and our in vivo imaging studies revealed that CeA<sub>GA</sub> neurons contain a heterogeneous population of neurons. We found that CeA<sub>GA</sub> neurons do not express *Sst*, *Pdyn* and *Nts*; however, a subset of CeA<sub>GA</sub> neurons expresses *Penk1* or *Pkc-d* (but *Penk1*<sup>+</sup> and *Pkc-d*<sup>+</sup> neurons represent a larger population of CeA neurons). We should note that *Pkc-d*<sup>+</sup> CeA neurons located in the capsular part of the CeA are involved in processing noxious and other aversive signals and can elicit defensive behaviors<sup>9,46–48</sup>, whereas *Pkc-d*<sup>+</sup> CeA neurons in the later division inhibit defensive behaviors<sup>8,49</sup> and inhibit feeding in response to a positive state, such as satiety<sup>9,49</sup>. We found that many CeA<sub>GA</sub> neurons expressing *Pkc-d* and activating CeA<sub>GA</sub> neurons inhibited pain responses, exactly opposite to the effect of activating *Pkc-d*<sup>+</sup> capsular CeA neurons<sup>46</sup>. Future work is needed to find additional markers to separate anti- versus pro-nociception *Pkc-d* cells. Neither *Pkc-d* nor *Penk1* nor both markers could define CeA<sub>GA</sub>. Although it is possible that a specific subset of CeA<sub>GA</sub> neurons exerts most of the analgesic function, it is also possible that the entire heterogeneous ensemble of CeA<sub>GA</sub> neurons as delineated by Fos<sup>+</sup> is required to work together to suppress pain. We observed widespread projections of CeA<sub>GA</sub> neurons to many regions activated by painful stimuli (Fig. 6). It is likely that different subpopulations of CeA<sub>GA</sub> innervate only a subset of these pain-processing centers, and the entire ensemble of CeA<sub>GA</sub> neurons is needed to carry out the full analgesic functions.

We also want to highlight the finding in the neuropathic orofacial pain model, in which nerve injury is well known to cause mechanical hypersensitivity. Under the conditions of CeA<sub>GA</sub> neuron activation, we found that the injured side was significantly less responsive (i.e. hyposensitive) to the normally painful 1.0 g von Frey filament (Fig. 5). This result is consistent with the fact that ligation injury damaged the nerve and thereby impaired the peripheral endings' ability to detect mechanical stimuli. This finding strongly suggests that the commonly observed tactile allodynia in neuropathic pain is likely due to altered central processing of signals transduced by spared uninjured sensory fibers. Activation of CeA<sub>GA</sub> neurons can suppress such abnormal central processing. We further observed that all of the CeA<sub>GA</sub> target regions contained neurons strongly activated by painful stimuli, and, remarkably, all such pain-elicited activity can be suppressed by concurrent optogenetic stimulation of CeA<sub>GA</sub> (Fig. 7). Interestingly, CeA<sub>GA</sub> neurons did not project to sensory thalamus, or to primary or secondary somatosensory cortex (data not shown), suggesting that these neurons likely function to dissociate pain perception from sensation, which was exactly the observed effect of low-dose ketamine on human patients<sup>3–5</sup>.

At present, we do not know how general anesthetics induce transient or sustained activation of CeA<sub>GA</sub> neurons. We also do not know whether persistently activating CeA<sub>GA</sub> neurons will be non-addictive. Nevertheless, our work raises the exciting possibility of harnessing the power of this endogenous analgesic system to relieve chronic pain. Future work aimed at identifying small molecular compounds that can specifically activate these powerful

analgesic neurons without the sedative effects of GA drugs could be developed into the next generation of painkillers.

### Online content

Any methods, additional references, Nature Research reporting summaries, source data, extended data, supplementary information, acknowledgements, peer review information; details of author contributions and competing interests; and statements of data and code availability are available at <https://doi.org/10.1038/s41593-020-0632-8>.

Received: 20 May 2019; Accepted: 30 March 2020;

Published online: 18 May 2020

### References

1. Aranake, A. et al. Increased risk of intraoperative awareness in patients with a history of awareness. *Anesthesiology* **119**, 1275–1283 (2013).
2. Sebel, P. S. et al. The incidence of awareness during anesthesia: a multicenter United States study. *Anesth. Analg.* **99**, 833–839 (2004).
3. Bergman, S. A. Ketamine: review of its pharmacology and its use in pediatric anesthesia. *Anesth. Prog.* **46**, 10–20 (1999).
4. Sadove, M. S., Shulman, M., Hatano, S. & Fevold, N. Analgesic effects of ketamine administered in subdissociative doses. *Anesth. Analg.* **50**, 452–457 (1971).
5. Gorlin, A. W., Rosenfeld, D. M. & Ramakrishna, H. Intravenous sub-anesthetic ketamine for perioperative analgesia. *J. Anaesthesiol. Clin. Pharmacol.* **32**, 160–167 (2016).
6. Brown, E. N., Purdon, P. L. & Van Dort, C. J. General anesthesia and altered states of arousal: a systems neuroscience analysis. *Annu. Rev. Neurosci.* **34**, 601–628 (2011).
7. Jiang-Xie, L.-F. et al. A common neuroendocrine substrate for diverse general anesthetics and sleep. *Neuron* **102**, 1053–1065 (2019).
8. Haubensak, W. et al. Genetic dissection of an amygdala microcircuit that gates conditioned fear. *Nature* **468**, 270–276 (2010).
9. Kim, J., Zhang, X., Muralidhar, S., LeBlanc, S. A. & Tonegawa, S. Basolateral to central amygdala neural circuits for appetitive behaviors. *Neuron* **93**, 1464–1479 (2017).
10. Choi, H. M. T. et al. Third-generation in situ hybridization chain reaction: multiplexed, quantitative, sensitive, versatile, robust. *Development* **145**, dev165753 (2018).
11. Sakurai, K. et al. Capturing and manipulating activated neuronal ensembles with cane delineates a hypothalamic social-fear circuit. *Neuron* **92**, 739–753 (2016).
12. Rodriguez, E. et al. A craniofacial-specific monosynaptic circuit enables heightened affective pain. *Nat. Neurosci.* **20**, 1734–1743 (2017).
13. McCullough, K. M., Morrison, F. G., Hartmann, J., Carlezon, W. A. & Ressler, K. J. Quantified coexpression analysis of central amygdala subpopulations. *eNeuro* **5**, ENEURO.0010-18.2018 (2018).
14. Sadler, K. E. et al. Divergent functions of the left and right central amygdala in visceral nociception. *Pain* **158**, 747–759 (2017).
15. Ji, G. & Neugebauer, V. Hemispheric lateralization of pain processing by amygdala neurons. *J. Neurophysiol.* **102**, 2253–2264 (2009).
16. Baas, D., Aleman, A. & Kahn, R. S. Lateralization of amygdala activation: a systematic review of functional neuroimaging studies. *Brain Res. Brain Res. Rev.* **45**, 96–103 (2004).
17. Lu, J. et al. MINIPIPE: A miniscope 1-photon-based calcium imaging signal extraction pipeline. *Cell Rep.* **23**, 3673–3684 (2018).
18. Sheintuch, L. et al. Tracking the same neurons across multiple days in Ca<sup>2+</sup> imaging data. *Cell Rep.* **21**, 1102–1115 (2017).
19. Boyden, E. S., Zhang, F., Bamberg, E., Nagel, G. & Deisseroth, K. Millisecond-timescale, genetically targeted optical control of neural activity. *Nat. Neurosci.* **8**, 1263–1268 (2005).
20. Chow, B. Y. et al. High-performance genetically targetable optical neural silencing by light-driven proton pumps. *Nature* **463**, 98–102 (2010).
21. Huang, T. et al. Identifying the pathways required for coping behaviours associated with sustained pain. *Nature* **565**, 86–90 (2019).
22. Hunskaar, S. & Hole, K. The formalin test in mice: dissociation between inflammatory and non-inflammatory pain. *Pain* **30**, 103–114 (1986).
23. Basbaum, A. I., Bautista, D. M., Scherrer, G. & Julius, D. Cellular and molecular mechanisms of pain. *Cell* **139**, 267–284 (2009).
24. Ding, W. et al. An improved rodent model of trigeminal neuropathic pain by unilateral chronic constriction injury of distal infraorbital nerve. *J. Pain* **18**, 899–907 (2017).
25. Giglio, J. A. & Gregg, J. M. Development of mirror pain following trigeminal nerve injury: a case report and review of neuropathic mechanisms. *Gen. Dent.* **66**, 27–32 (2018).

26. Milligan, E. D. et al. Spinal glia and proinflammatory cytokines mediate mirror-image neuropathic pain in rats. *J. Neurosci.* **23**, 1026–1040 (2003).
27. Cai, Y.-Q., Wang, W., Paulucci-Holthauzen, A. & Pan, Z. Z. Brain circuits mediating opposing effects on emotion and pain. *J. Neurosci.* **38**, 6340–6349 (2018).
28. Han, S., Soleiman, M. T., Soden, M. E., Zweifel, L. S. & Palmiter, R. D. Elucidating an affective pain circuit that creates a threat memory. *Cell* **162**, 363–374 (2015).
29. Wang, D. et al. Functional divergence of  $\Delta$  and  $\mu$  opioid receptor organization in CNS pain circuits. *Neuron* **98**, 90–108.e5 (2018).
30. Corder, G. et al. An amygdalar neural ensemble that encodes the unpleasantness of pain. *Science* **363**, 276–281 (2019).
31. Levin-Arama, M. et al. Subcutaneous compared with intraperitoneal ketamine–xylazine for anesthesia of mice. *J. Am. Assoc. Lab. Anim. Sci.* **55**, 794–800 (2016).
32. Beecher, H. K. Pain in men wounded in battle. *Bull. US Army Med. Dep.* **5**, 445–454 (1946).
33. Petrovic, P., Kalso, E., Petersson, K. M. & Ingvar, M. Placebo and opioid analgesia—imaging a shared neuronal network. *Science* **295**, 1737–1740 (2002).
34. Benedetti, F. Placebo and endogenous mechanisms of analgesia. *Handb. Exp. Pharmacol.* 393–413 (2007).
35. Eippert, F. et al. Activation of the opioidergic descending pain control system underlies placebo analgesia. *Neuron* **63**, 533–543 (2009).
36. Basbaum, A. I. & Fields, H. L. Endogenous pain control systems: brainstem spinal pathways and endorphin circuitry. *Annu. Rev. Neurosci.* **7**, 309–338 (1984).
37. Ossipov, M. H., Dussor, G. O. & Porreca, F. Central modulation of pain. *J. Clin. Invest.* **120**, 3779–3787 (2010).
38. Lau, B. K. & Vaughan, C. W. Descending modulation of pain: the GABA disinhibition hypothesis of analgesia. *Curr. Opin. Neurobiol.* **29**, 159–164 (2014).
39. Butler, R. K. & Finn, D. P. Stress-induced analgesia. *Prog. Neurobiol.* **88**, 184–202 (2009).
40. Wager, T. D., Scott, D. J. & Zubieta, J.-K. Placebo effects on human  $\mu$ -opioid activity during pain. *Proc. Natl Acad. Sci. USA* **104**, 11056–11061 (2007).
41. Werka, T. & Marek, P. Post-stress analgesia after lesions to the central nucleus of the amygdala in rats. *Acta Neurobiol. Exp.* **50**, 13–22 (1990).
42. Duvarci, S. & Pare, D. Amygdala microcircuits controlling learned fear. *Neuron* **82**, 966–980 (2014).
43. Herry, C. & Johansen, J. P. Encoding of fear learning and memory in distributed neuronal circuits. *Nat. Neurosci.* **17**, 1644–1654 (2014).
44. Neugebauer, V. Amygdala pain mechanisms. *Handb. Exp. Pharmacol.* **227**, 261–284 (2015).
45. Parikh, D. et al. Stress-induced analgesia and endogenous opioid peptides: the importance of stress duration. *Eur. J. Pharmacol.* **650**, 563–567 (2011).
46. Wilson, T. D. et al. Dual and opposing functions of the central amygdala in the modulation of pain. *Cell Rep.* **29**, 332–346 (2019).
47. Yu, K. et al. The central amygdala controls learning in the lateral amygdala. *Nat. Neurosci.* **20**, 1680–1685 (2017).
48. Cui, Y. et al. A central amygdala–substantia innominata neural circuitry encodes aversive reinforcement signals. *Cell Rep.* **21**, 1770–1782 (2017).
49. Cai, H., Haubensak, W., Anthony, T. E. & Anderson, D. J. Central amygdala PKC- $\delta^+$  neurons mediate the influence of multiple anorexigenic signals. *Nat. Neurosci.* **17**, 1240–1248 (2014).

**Publisher's note** Springer Nature remains neutral with regard to jurisdictional claims in published maps and institutional affiliations.

© The Author(s), under exclusive licence to Springer Nature America, Inc. 2020

## Methods

**Animal statement.** All experiments were conducted according to protocols approved by the Duke University Institutional Animal Care and Use Committee.

**Animals.** Adult male and female (more than 8 weeks old) Fos<sup>TVA</sup> mice (Jackson Laboratory, stock no. 027831) were used for all experiments. Mice were housed in the vivarium with a 12-h light/dark cycle and were given food and water ad libitum. vGAT-IRES-cre mice (Jackson Laboratory, stock no. 016962) were used for some immunohistochemistry experiments.

**Viruses.** CANE-LV-Cre (titer,  $5 \times 10^8$  ifu per ml; CANE-LV envelope (Addgene, plasmid no. 86666)) were produced as previously described. Various AAVs were co-injected with CANE-LV-Cre: AAV2/1-CAG-Flex-GFP (UNC Vector Core), AAV2/1-CBA-Flex-ChR2-mCherry (UPenn Vector Core), AAV2/1-hSyn-ChR2(H134R)-eYFP (UPenn Vector Core and Addgene), AAV2/1-Efla-DIO-eArch-eYFP (Addgene) and AAV2/1-CAG-Flex-GCaMP6m (Addgene).

**Surgical procedures. Viral delivery.** To capture and express desired transgenes in CeA<sub>GA</sub> neurons, Fos<sup>TVA</sup> mice were anesthetized with isoflurane (1.5% isoflurane and 0.75% oxygen) for 2 h (to induce Fos expression in CeA<sub>GA</sub>) in a chamber before mice were transported to a stereotaxic frame (David Kopf Instruments), and small craniotomies were created over the target region. The coordinates of CeA used relative to bregma were as follows: AP = 1.15 or  $1.20 \pm 0.05$  mm, ML = 2.83 or  $2.86 \pm 0.02$  mm, DV =  $-4.17$  or  $-4.22 \pm 0.03$  mm. The CANE-LV-Cre and Cre-dependent AAV were mixed (1:1) before injection. One  $\mu$ l total was delivered at a rate of 60 nl min<sup>-1</sup> per injection and left for 10 min after injection for efficient diffusion of the virus.

**Optic fiber implantation.** After viral injection, an optical fiber (200- $\mu$ m core diameter, Thorlabs) was inserted 300  $\mu$ m above the injection site and secured using Metabond (Parkell) and dental cement. During post hoc immunohistochemical analysis, viral expression, site of injection and insertion of optical fiber were confirmed; animals with failed expression or off-target optical fiber placement were excluded from all analysis.

**EEG/EMG and CeA<sub>GA</sub> optogenetic experimental procedure.** Three stainless steel screws were placed on the left frontal, left parietal and right cerebellar cortex as EEG electrodes, and two headmount-coupled stainless steel leads (8201-SS, Pinnacle Technology) were inserted into bilateral neck muscles as electromyography (EMG) electrodes. For optogenetic activation, one optical fiber was inserted on top of the right CeA. All three EEG electrodes were further connected onto the headmount (8201-SS, Pinnacle Technology). EEG and EMG were recorded with Sirenia Acquisition (Pinnacle Technology) at 1,000 Hz. For optogenetic experiments, after 5 min of recorded EEG baseline in the recording chamber, three laser trains (20 Hz, 20 ms and 2 min on followed by 2 min off, ~4 mW from the fiber tip, 473-nm blue laser) were given per experimental animal.

**GRIN lens implantation and baseplate attachment.** A GRIN lens (7.3  $\times$  0.6 mm, Inscopix) was implanted according to manufacturer instructions. A holder (Inscopix, gripper part ID: 1050-002199) was used to lower the miniature microscope with the baseplate onto the top of the GRIN lens until the GCaMP6m fluorescence was visible under the illumination from the miniscope's LED. Subsequently, the baseplate was fixed to the skull with dental cement darkened with carbon powder to prevent external light from contaminating the imaging field of view. A cover (Inscopix, part ID: 1050-002193) was attached to the baseplate to protect the microendoscope.

**CCI-IoN.** Animals were anesthetized with K/X, and a small incision (~0.35 cm) parallel to the midline was made starting at the caudal end of the third row of whiskers toward the ipsilateral orbit. The superficial fascia was gently separated to expose the IoN trunk at its distal segment outside the orbital cavity. Two chromic ligatures (6-0, Angiotech) were loosely tied around the distal part of the IoN (1 mm apart). The wound was checked for hemostasis, and the incision was closed with three 5-0 silk sutures (Angiotech).

**In vivo optogenetic activation or silencing.** Animals with optical fiber implants were connected to an optical patch cable (Thorlabs) coupled to either a 473-nm or a 561-nm laser (Opto Engine). Light pulse was controlled by a pulse generator (Master 8 or AMi-2 Optogenetic Interface). Next, a 473-nm laser was applied in pulsed mode (~3.5 mW/mm<sup>2</sup>, 20 Hz, 20-ms pulse width) to animals that expressed ChR2 in CeA<sub>GA</sub> and their respective GFP controls, whereas a 561-nm laser was applied in continuous mode (~15 mW/mm<sup>2</sup>) to animals that expressed eArch in CeA<sub>GA</sub> and their respective GFP controls.

**Immunohistochemical analysis.** To detect GA-activated neurons, animals were anesthetized with isoflurane or K/X or Dex for 2 h and then transcardially perfused with 10% sucrose in cold phosphate-buffered saline (PBS, pH 7.4) followed by 4% cold paraformaldehyde fixation solution. To detect restraint

stress-activated neurons, mice were placed in the restrainer for 90 min (TV-150, Braintree Scientific). All brains were post-fixed in paraformaldehyde overnight at 4°C, cryoprotected in 30% sucrose PBS solution for 2–3 d at 4°C, frozen in O.C.T compound (Tissue-Tek, Sakura) and then stored at –80°C until sectioning. Floating brain sections (80  $\mu$ m) were stained using standard immunofluorescent protocol. The primary antibodies used were as follows: goat anti-Fos (Santa Cruz Biotechnology, sc520g, 1:300)<sup>50</sup>, rabbit anti-Fos (Cell Signaling, 2250, 1:1,500)<sup>51</sup> and anti-neurotensin (ImmunoStar, 20072)<sup>52</sup>. The secondary antibodies used were: Alexa Fluor 488 donkey anti-goat (Jackson ImmunoResearch, 705-545-147, 1:500)<sup>53</sup>, Alexa Fluor 647 anti-rabbit (Jackson ImmunoResearch, 711-605-152, 1:500)<sup>54</sup> and Cy3 donkey anti-goat (Jackson ImmunoResearch, 705-165-147, 1:500)<sup>55</sup> (see Life Sciences Reporting Summary).

**Fluorescence in situ hybridization.** For each brain collected, after 1 h of isoflurane anesthesia, 8–10 slices (60- $\mu$ m thick) containing the CeA were collected, and fluorescence in situ hybridization was performed as described previously<sup>11</sup>. *Penk1*, *Pkc-d*, *Pdyn*, *Sst* and *Fos* probes were the same as the ones used by the Allen Brain Atlas. Fluorescein isothiocyanate-labeled (FITC) *Fos* probe was paired with digoxigenin-labeled (DIG) *Penk1*, *Pkc-d*, *Pdyn* or *Sst* probes to analyze the co-localization of *Fos* with these markers.

**Three-color HCR in situ hybridization to examine *Fos*, *Penk1* and *Pkc-d* expression.** HCR in situ hybridization was performed as described<sup>10</sup>. Probes were ordered from Molecular Instruments. For each brain collected, after 1 h of isoflurane anesthesia, 8–10 slices (60- $\mu$ m thick) containing the CeA were collected and hybridization chain reaction in situ was performed. On day 1, collected brain slices were exposed to probe hybridization buffer with HCR Probe Set. On day 2, brain slices were washed with probe wash buffer and received amplification buffer and amplifier. On day 3, brain slices were counterstained with DAPI and mounted. *Penk1* (488 nm), *Pkc-d* (647 nm) and *Fos* (546 nm) probes were used to examine any overlaps between these markers.

**Histologic image acquisition and quantification. Image acquisition.** Brain slices were visualized with a laser scanning confocal microscope (Zeiss 700). Entire brain slices were imaged at  $\times 10$  resolution, whereas the entire CeA was imaged at  $\times 20$  resolution using z stack (~30  $\mu$ m). Cells were manually quantified for co-localization and total Fos count between *Fos*-expressing neurons and respective markers by a researcher blinded to the samples. For each animal, six slices were averaged for the entire CeA region before averaging percentages across all animals.

**Projection average intensity values.** The regions of interest (ROIs) and borders for each region were drawn according to the Allen Brain Atlas. The mean, or average intensity value, was calculated for each region using the histogram function in Photoshop. The mean value was recorded across all samples, and an average was computed across three samples.

**Behavioral tests. Formalin injection.** Formalin (Sigma, 37%) was diluted to 4% with PBS, and 10  $\mu$ l was unilaterally injected into the top of the hind paw or the whisker pad to induce inflammatory pain. The animals displayed self-recuperating behavior dependent on injection site, such as licking of the hind paw or wiping of the whisker pad. Formalin injection induced two distinct phases of acute pain. Self-recuperating behavior was video-recorded immediately after injection. During the first and second phase, optogenetic stimulation was initiated for 2-min-on and -off periods for three (first phase, 6-min stimulation) and six (second phase, 12-min stimulation) times. Self-recuperating behavior was recorded and analyzed.

**Spontaneous wiping behavior.** After CCI-IoN, animals exhibited spontaneous wiping behavior as a result of the injury. Animals were placed into a clear cylindrical chamber and attached to the patch cable. Each animal was placed in the chamber and video-recorded for 19 min (7-min baseline, 5-min stimulation and 7-min post-stimulation). Optogenetic illumination was turned on during the middle 5-min period, and total time exhibiting spontaneous wiping behavior was measured.

**Low-dose ketamine analgesia experiments.** Mice were injected with 12 mg kg<sup>-1</sup> of ketamine and placed back into their home cage for 6 min. Then, mice were given an injection of 10  $\mu$ l of 0.2- $\mu$ g  $\mu$ l<sup>-1</sup> capsaicin (capsaicin was diluted with from a 10- $\mu$ g  $\mu$ l<sup>-1</sup> stock to 0.2  $\mu$ g  $\mu$ l<sup>-1</sup> in saline with 4% ethanol and 4% Tween –80). Mice were immediately video-recorded for 15 min in a cylinder plexiglass container. Mice with optogenetic silencing received silencing during the first (0–5 min) and last (10–15 min) 5-min bins. The total licking time was computed from the entire 15 min of recording as the animals exhibited self-recuperating behavior by licking the hind paw.

**Hargreaves heat test.** To examine thermal sensitivity, animals were placed in the Hargreaves test enclosure for 5–10 min to acclimate. The guiding lines were used to position the infrared emitter/detector directly underneath the plantar region of the hind paws. The infrared intensity was set to 40. The reaction time was recorded. Each animal received three trials per hind paw, each applied at least 30 s apart.

**Cold dry ice test.** To examine cold sensitivity, animals were placed in a 13 × 13 × 20-cm chamber that was raised 30.5 cm above the floor and left to acclimate for 5–10 min. The floor of the chamber was a 0.80-mm-thick polycarbonate sheet. Dry ice was pounded into a fine powder and packed tightly into a 0.5-inch-diameter syringe to form a cylindrical shape. Dry ice was pushed out of the syringe and centered on the plantar region of the hind paws. The syringe was promptly removed after the animal displayed a withdrawal reflex. Withdrawal behavior was video-recorded. Each animal received three trials per hind paw, each applied at least 10 s apart.

**von Frey test on the face.** To assess mechanical sensitivity, animals received ten repeated application (10–20 s apart) of various von Frey filaments with increasing forces (0.008–1 g) to the whisker pads (with all whiskers kept intact). In the CCI-IoN model, filaments were applied near the ligation injury. ‘Withdrawal Threshold’ was defined as the first filament that induced withdrawal latency over 50% of the ten repeated applications.

**von Frey test on the paw.** To assess mechanical sensitivity, animals received ten repeated application (10–20 s apart) of various von Frey filaments with increasing forces (0.40–4.0 g) to the hind paws.

**Electronic von Frey test on the hind paws.** The electronic von Frey (eVF) test was used exclusively for the hind paws. The eVF rigid tip was applied to the plantar region of the hind paws, and the withdrawal threshold was recorded. The calibration was set at reaching 50 g in 5 s. Each animal received three trials per hind paw, each applied at least 10–20 s apart.

**Open field test.** To assess locomotion and anxiety-like behavior, animals were placed in a 30 × 30-cm box. Each animal was placed in the center of the box, and locomotion activity and freezing behavior was recorded for a total of 15 min. Animals were attached to the patch cable and optogenetic illumination was turned on during the middle 5-min period. ANY-maze software (Stoelting) was used to create a 15 × 15-cm center zone within the box and also used to analyze the video-recording.

**EPM test.** To assess anxiety-like behavior to optogenetic illumination of the CeA, mice were placed in an EPM for 15 min. Animals were attached to the patch cable and received optogenetic illumination during the middle 5-min period. Locomotion and time spent in the open and closed arms were analyzed and recorded using ANY-maze software.

**CPP and CPA tests.** To determine if optogenetic activation or silencing of CeA<sub>GA</sub> induced a place preference or aversion, animals were placed in a two-chamber 20 × 40-cm box and attached to a patch cable. Each chamber contained two distinct visual patterns of horizontal and vertical stripes. On day 1, animals were placed in the center of the box and left to explore the box without illumination for 10 min. The preference of the animal was determined by the chamber the animal spent more time in. For the next 4 d (days 2–5), animals received illumination on days 3 and 5 and no illumination on days 2 and 4. On the last day (day 6), animals could freely explore the two chambers to determine the new place preference without illumination. Chr2-expressing animals received illumination on the side they did not prefer for 22 min with 2-min-on and 2-min-off periods, whereas eArch-expressing animals received illumination on the side they did prefer for 10 min continuously. This test was designed to bias against the animal's natural preference. ANY-maze software was used to analyze the time spent in each chamber.

In a separate experiment, CCI-IoN animals expressing Chr2 or GFP controls were also placed in the same two-chamber box to determine if optogenetic activation of CeA<sub>GA</sub> altered the natural place preference in a state of chronic pain.

**Ultrasonic vocalization and courtship behavior.** Male animals were placed in a clear cylindrical chamber with estrus female BL6 animals for 90 s (baseline), and then male animals received optogenetic stimulation for 90 s. Male ultrasonic vocalizations were recorded with an ultrasonic microphone (CM16/CMPA-P48, Avisoft Bioacoustics) and analyzed with MUPET<sup>®</sup>. Courtship behavior was defined as anogenital sniffing and mounting. Behavior was video-recorded, and the differences of total syllables elicited during ultrasonic vocalizations and the duration of courtship behavior with and without light stimulation were quantified.

**In vivo calcium imaging and image data analyses.** Next, we did calcium imaging recordings of CANE<sub>ISO</sub>-GCaMP6m CeA<sub>GA</sub> neurons in behavioral experiments. After the baseplate attachment, each CANE<sub>ISO</sub>-GCaMP6m CeA<sub>GA</sub> mouse was acclimated to handling and attachment of the Inscopix miniature microscope for 10–15 min per day for 3–5 d. A Doric TTL Pulse Generator (Doric, OTPG\_4) was used to trigger and synchronize behavioral video-recordings with calcium recordings.

**Part 1, anesthesia and noxious stimuli test.** We first imaged neural activities during re-exposure to isoflurane-induced anesthesia (day 1, 5-min baseline

followed by 20 min of 1.5% isoflurane mixed with oxygen). On day 3, we imaged the neurons during K/X-induced anesthesia (5-min baseline followed by i.p. injection of ketamine (100 mg kg<sup>-1</sup>) and xylazine (10 mg kg<sup>-1</sup>) and imaged for 20 min continuously). On days 5–8, we imaged the neurons before, during and after applications of noxious stimuli (dry ice, heat, von Frey on hind paw and von Frey on facial pad), with a 1-d interval between each sensory test experiment. Two days after, we repeated imaging of neural activities in some mice during 1.5% isoflurane- (day 10) and K/X- (day 12) induced anesthesia. Seven mice underwent imaging under anesthesia, six underwent cold and heat stimuli and four underwent von Frey stimuli on the hind paws and facial pads.

**Part 2, anesthesia and stress.** Calcium imaging recordings of restraint stress (8-min baseline followed by 8-min restriction with AIMS rodent restraint bags and, later, 8-min release from the restriction) and isoflurane anesthesia (1.5%, 5-min baseline followed by 20 min of 1.5% isoflurane mixed with oxygen) were done separately within 1 d (day 1). Then, on day 3, we imaged neurons during low-dose ketamine (5-min baseline followed by i.p. injection of ketamine (12 mg kg<sup>-1</sup>) and imaged for 20 min continuously) and regular-dose ketamine on day 4 (5-min baseline followed by i.p. injection of ketamine (100 mg kg<sup>-1</sup>) and imaged for 20 min continuously). On day 6, we imaged neurons during low-dose isoflurane (0.5%, 5-min baseline followed by 20 min of 0.5% isoflurane mixed with oxygen). Mice moved around under low-dose ketamine and low-dose isoflurane administration. On day 8, we repeated imaging recordings of restraint stress and isoflurane- (1.5%) induced anesthesia separately. Five mice went through this series of imaging.

**Imaging data analysis.** All the calcium imaging data were processed from the raw video by MINPIPE<sup>17</sup>, where videos underwent background subtraction, movement correction, automatic seeds selection and ROI separation. The extracted ROIs were then manually inspected again by experienced researchers to ensure that only the most reliable units were included. The traces of the refined set of ROIs were then rescaled to the same range (between 0 and 1 with arbitrary unit).

For the isoflurane and ketamine experiments, the refined traces were aligned according to the delivery moment of the anesthetics, and the window from 4 min before (baseline, –4 to 0 min) to 20 min after (isoflurane or ketamine, 0–20 min) the delivery moment was selected to perform data analysis. The aligned traces were sorted by the average calcium fluorescence intensity ratio of all the units, first sorted by (isoflurane or ketamine period) / (baseline) (Fig. 2c,e), and then sorted by (last 10 min of isoflurane or ketamine) / (first 10 min of isoflurane/ ketamine) (Fig. 2d,f). The sorted traces were roughly classified into isoflurane- or ketamine-active and suppressed groups (Fig. 2c,e) or sustained, transient and suppressed groups (Fig. 2d,f and Extended Data Fig. 2d,e), respectively, where the average trace of each group was calculated. To further examine the finer dynamic property of different groups, the percentage contribution of the last 10 min to the overall 24-min duration of each trace was calculated. The distribution of the sustained activity and transient activity in percentage contribution was then calculated from each group or each mouse.

To evaluate the isoflurane and ketamine neural response, we in general applied four approaches, including direct calculation and corrected calculation (Fig. 2h, right, Extended Data Fig. 2f,g). The direct calculation method is computing the ratio of the mean activity for stimulus ON (isoflurane or ketamine delivery) and OFF (baseline) periods, indicated by mean / mean, where activity in the stimulus ON period might be underestimated owing to the changes of brain dynamics during the long imaging time window over anesthesia (20 min). Therefore, we also calculated the corrected (effective) mean intensity (Eff.) for the ON and/or OFF periods (Eff. / Eff. or Eff. / mean) before computing the ON/OFF activity ratio, by computing only the average activity during the time when the calcium intensity was at least two median absolute deviations above the overall mean. In addition, we calculated the effective active duration of individual neurons. Neurons with effective active time over a certain amount of time (1 min) after stimulus ON (anesthesia onset) could be considered as activated by the stimulus (Eff. time).

In the sensory stimuli application experiments (Fig. 4), for every stimulus applied in these experiments, a trial was defined with a window of 10 s before and 10 s after the stimulus. All the traces from the same experimental condition were epoched based on the trials and were then pooled together and sorted by the peak activity latency within the trial. The mean activity trace was calculated by averaging across the epoched traces of all neurons and all trials. For each individual neuron, the sorted traces from all trials of the same condition were further pooled together to show the neuronal response to the stimuli. To investigate the neuronal response change, the pooled traces were averaged, and the overall activity difference between the 5-s post-response average and the 5-s pre-response average was calculated for all individual neurons, on the basis of which empirical probability distribution was computed across neurons. To group the neurons on the basis of the response types, the activity difference of individual neurons was compared with a threshold of two times of the standard deviation of the averaged neuronal activity in that trial. If the activity difference was higher than the threshold, the neuron was considered to be in the activity-increased group; if the activity difference was lower than the negative of the threshold, the neuron was considered to be in the activity-suppressed group; otherwise the neuron was classified as being in the unchanged group. The proportion of each group was then calculated.

In the restraint stress experiment (Extended Data Fig. 3), the first 8 min was recorded for baseline spontaneous activity (−8 to 0 min); the second 8 min (0–8 min) was recorded when mice were under restraint; and the third 8 min (8–16 min) was recorded when mice were released from the restraint. To further characterize the stress responses and compare neuronal responses to stress and isoflurane (as shown in Extended Data Fig. 3e–h), we tracked the same neurons across stress and isoflurane sessions, computed the corrected/effective mean calcium intensity for the stress period (0–8 min) and two baseline periods (−8 to 0 min and 8–16 min). Only the time points when signal intensity was over two median absolute deviations above the mean were considered as effective time points. Then, we calculated the ratio between the corrected mean intensities for each neuron and labeled the neuron to be stress activated if the ratio was above 1 and labeled to be stress suppressed if the ratio was below 1. To further have a more conservative calculation, we excluded the neurons with maximum intensity below 0.1 (normalized intensity) over the whole duration. The remaining neurons were labeled as the robust group and used for later cross-analysis with isoflurane responses.

**Same-cell tracking (cross-day analysis) of  $CeA_{GA}$  calcium activity.** To register neurons across days from different calcium imaging recordings sessions of the same mouse, we adapted the CellReg method with the Log Demons registration method used in MIN1PIPE<sup>17,18</sup>. In brief, all the extracted ROIs from each session to be tracked were collected, and then the modified CellReg was applied. Only the ROIs that were reliably tracked were used for subsequent analyses.

**EEG analysis.** The EEG signal was first epoched to laser-on (2 min) and laser-off (2 min) periods, and the power spectrum was calculated using fast Fourier transform. The power spectrum was then normalized to the full-frequency band on which each epoch was valid, and only the band (0 and 20 Hz) was extracted to further compute the average trace across the nine epochs ( $n = 3$  mice, three repetitions in each mouse).

**Statistics.** All statistical analyses were performed in GraphPad Prism 8. Behavior data were analyzed with two-way ANOVA followed by Tukey's test, Sidak's test and Dunnett's post hoc multiple-comparison test when appropriate. All  $t$ -tests were performed as two-tailed. Significance levels are indicated as follows: \* $P < 0.05$ , \*\* $P < 0.01$ , \*\*\* $P < 0.001$  and \*\*\*\* $P < 0.0001$ , and precise  $P$  values are given when appropriate in Supplementary Table 1. Sample sizes were determined on the basis of previous publications in the lab and common practice in animal behavior experiments<sup>11,12,57,58</sup> (see Life Sciences Reporting Summary). We did not observe any sex-dependent differences in all our experiments; therefore, results from males and females were grouped and analyzed together. Data distribution was assumed to be normal, but this was not formally tested; instead, all graphs contain individual data points and mean  $\pm$  s.e.m.

**Randomization and data collection.** Animals were randomly assigned to various treatment groups to receive GFP control, channelrhodopsin or enhanced archaerhodopsin. A different experimenter, who was blinded to the conditions of the experiments, performed data analysis. All animals were used as data points, and animals were excluded from analysis only if they were incorrectly targeted virally.

**Reporting Summary.** Further information on research design is available in the Nature Research Reporting Summary linked to this article.

## Data availability

All raw data described in this study are available from the corresponding authors upon reasonable request. All codes described in this study are available from the corresponding authors upon reasonable request. The MIN1PIPE code for processing miniscope imaging (correspondence should be addressed to Jinghao Lu, jinghao.lu@duke.edu) is available at: <https://github.com/JinghaoLu/MIN1PIPE>.

## References

50. Venza, M. et al. The overriding of TRAIL resistance by the histone deacetylase inhibitor MS-275 involves  $c$ -myc up-regulation in cutaneous, uveal, and mucosal melanoma. *Int. Immunopharmacol.* **28**, 313–321 (2015).

51. Pang, D. et al. Polyphyllin II inhibits liver cancer cell proliferation, migration and invasion through downregulated cofilin activity and the AKT/NF- $\kappa$ B pathway. *Biol. Open* **9**, bio046854 (2020).
52. Faget, L. et al. Opponent control of behavioral reinforcement by inhibitory and excitatory projections from the ventral pallidum. *Nat. Commun.* **9**, 849 (2018).
53. Zamparo, I. et al. Axonal odorant receptors mediate axon targeting. *Cell Rep.* **29**, 4334–4348 (2019).
54. Hara, Y. et al. Anti-tumor effects of an antagonistic mAb against the ASCT2 amino acid transporter on KRAS-mutated human colorectal cancer cells. *Cancer Med.* **9**, 302–312 (2020).
55. Simon, C. M. et al. Stasimon contributes to the loss of sensory synapses and motor neuron death in a mouse model of spinal muscular atrophy. *Cell Rep.* **29**, 3885–3901.e5 (2019).
56. Van Segbroeck, M., Knoll, A. T., Levitt, P. & Narayanan, S. MUPET-Mouse ultrasonic profile extraction: a signal processing tool for rapid and unsupervised analysis of ultrasonic vocalizations. *Neuron* **94**, 465–485.e5 (2017).
57. Zhang, Y., Chen, Y., Liedtke, W. & Wang, F. Lack of evidence for ectopic sprouting of genetically labeled A $\beta$  touch afferents in inflammatory and neuropathic trigeminal pain. *Mol. Pain* **11**, 18 (2015).
58. Zhang, Y. et al. Identifying local and descending inputs for primary sensory neurons. *J. Clin. Invest.* **125**, 3782–3794 (2015).

## Acknowledgements

We thank J. Takatoh for helping with optimizing image compression that retains good resolution and for designing the color scheme for projection data. We also thank V. Prevosto and P. Thompson for helping with statistics and R. Mooney, R.-R. Ji and members of the Wang lab for critical reading of this manuscript. We thank the Janelia GENIE project for making GCaMP6m sensor available to the research community. Correspondence for calcium imaging data processing codes should be addressed to Jinghao Lu (jinghao.lu@duke.edu). T.H. is supported by the NSF GRFP scholarship. Y.C. is supported by R01 DE027454. This work is supported by NIH DP1MH103908, a Holland-Trice Scholar award, a W. M. Keck Foundation grant, NIH R01 NS109947 and NIH R01 DE029342.

## Author contributions

F.W. conceived the initial idea. F.W., T.H. and B.C. designed experiments with help from K.S. T.H. was responsible for immunohistochemical analysis, HCR in situ hybridization, all optogenetic manipulations during all types of sensory and affective behaviors and for generating and analyzing axon projection data. B.C. was responsible for all miniscope GCaMP6 imaging experiments under different conditions. J.L. was responsible for analysis of all imaging data and EEG data (blinded to experimental conditions). D.L. performed stress responses, mating experiments and EEG recordings and analyzed some of the behavioral data. K.S. performed some initial experiments. J.K. did some of the quantifications of histology and behavior results. S.Z. produced all CANE-LV viruses. S.Z. and D.L. performed some of the two-color molecular marker analysis. B.-X.H. took care of mouse husbandry and genotyping. L.Y. performed some slice recording experiments (data not shown). Y.C. performed chronic ligation surgeries. F.W., T.H. and B.C. wrote the manuscript with help from J.L.

## Competing interests

The authors declare no competing interests.

## Additional information

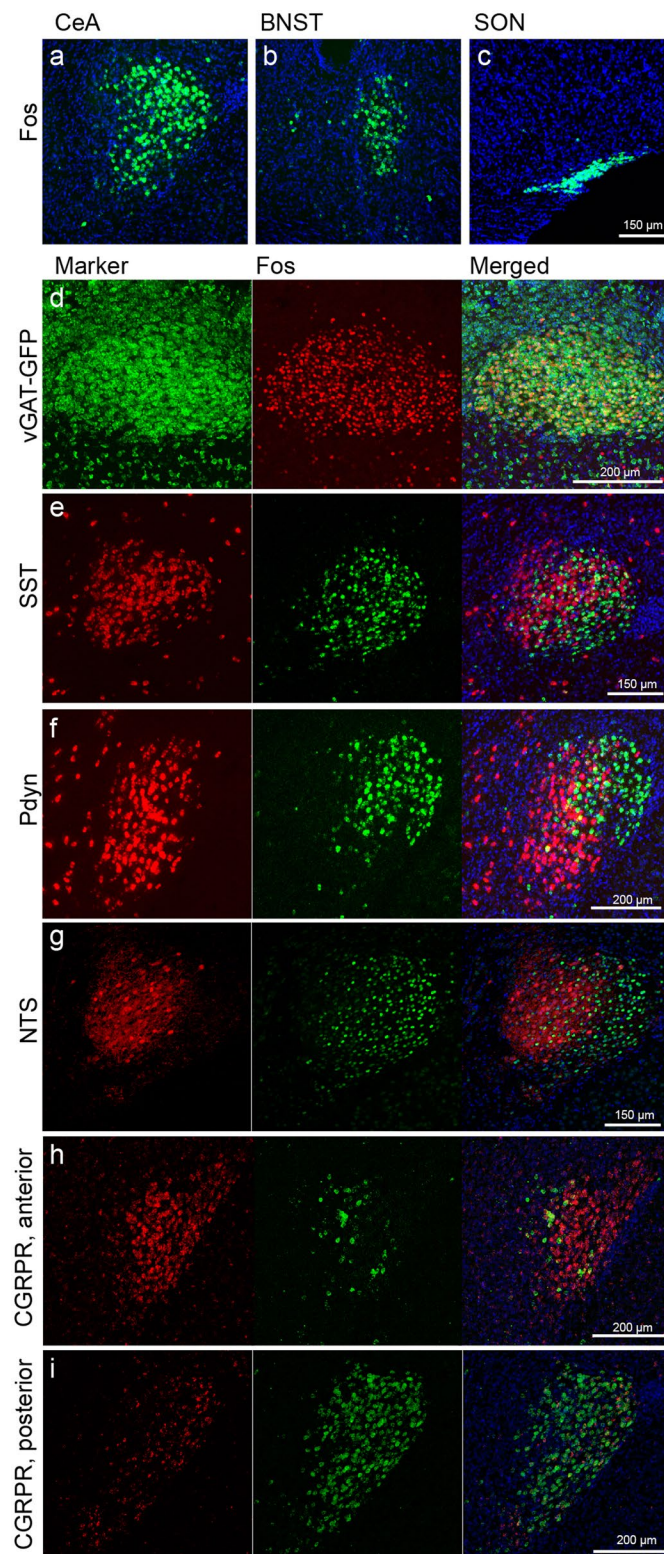
**Extended data** is available for this paper at <https://doi.org/10.1038/s41593-020-0632-8>.

**Supplementary information** is available for this paper at <https://doi.org/10.1038/s41593-020-0632-8>.

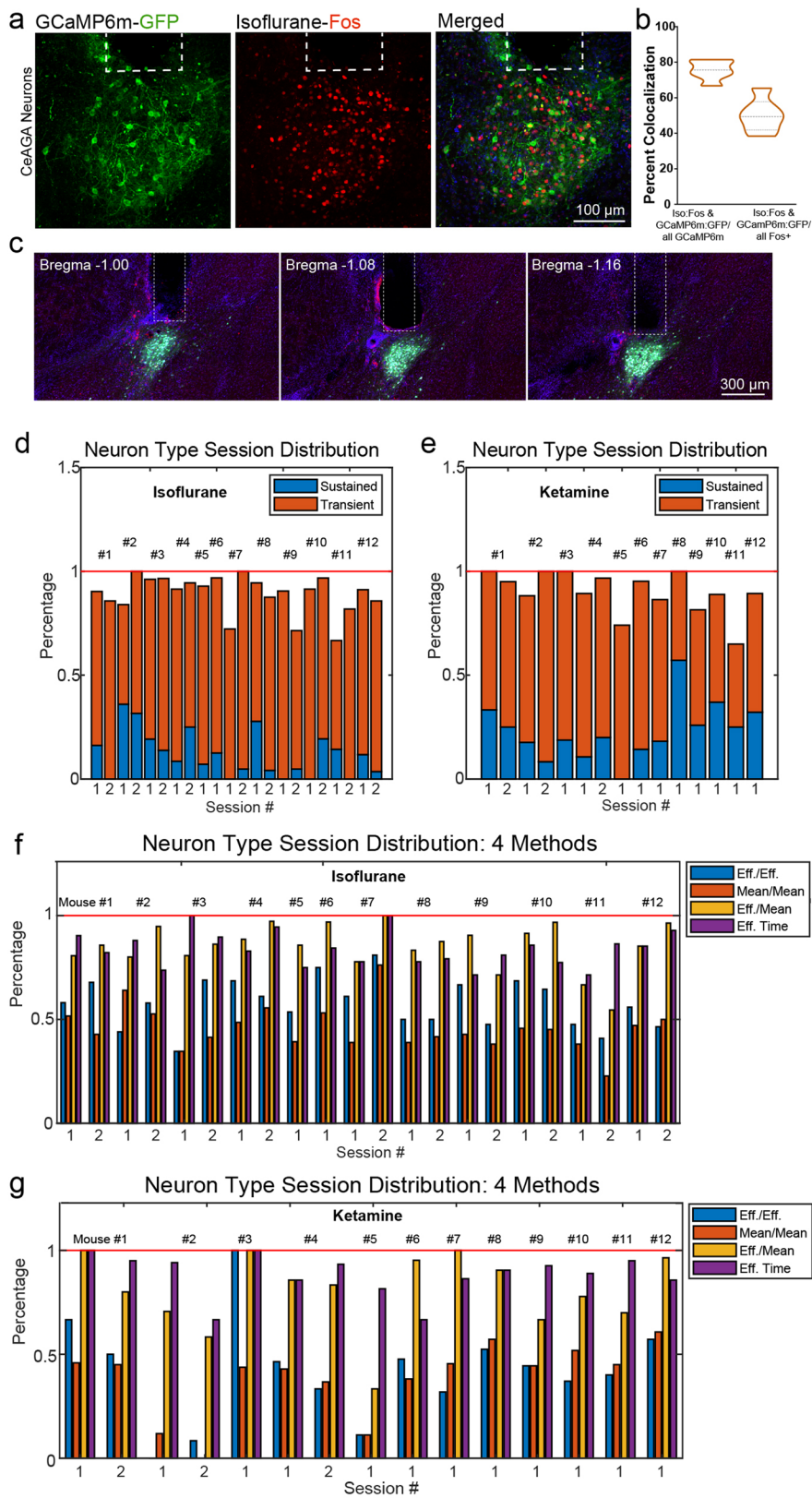
**Correspondence and requests for materials** should be addressed to T.H. or F.W.

**Peer review information** *Nature Neuroscience* thanks Gregory Corder, Nora McCall, Katelyn Sadler, Jessica Wojick and the other, anonymous, reviewer(s) for their contribution to the peer review of this work.

**Reprints and permissions information** is available at [www.nature.com/reprints](http://www.nature.com/reprints).

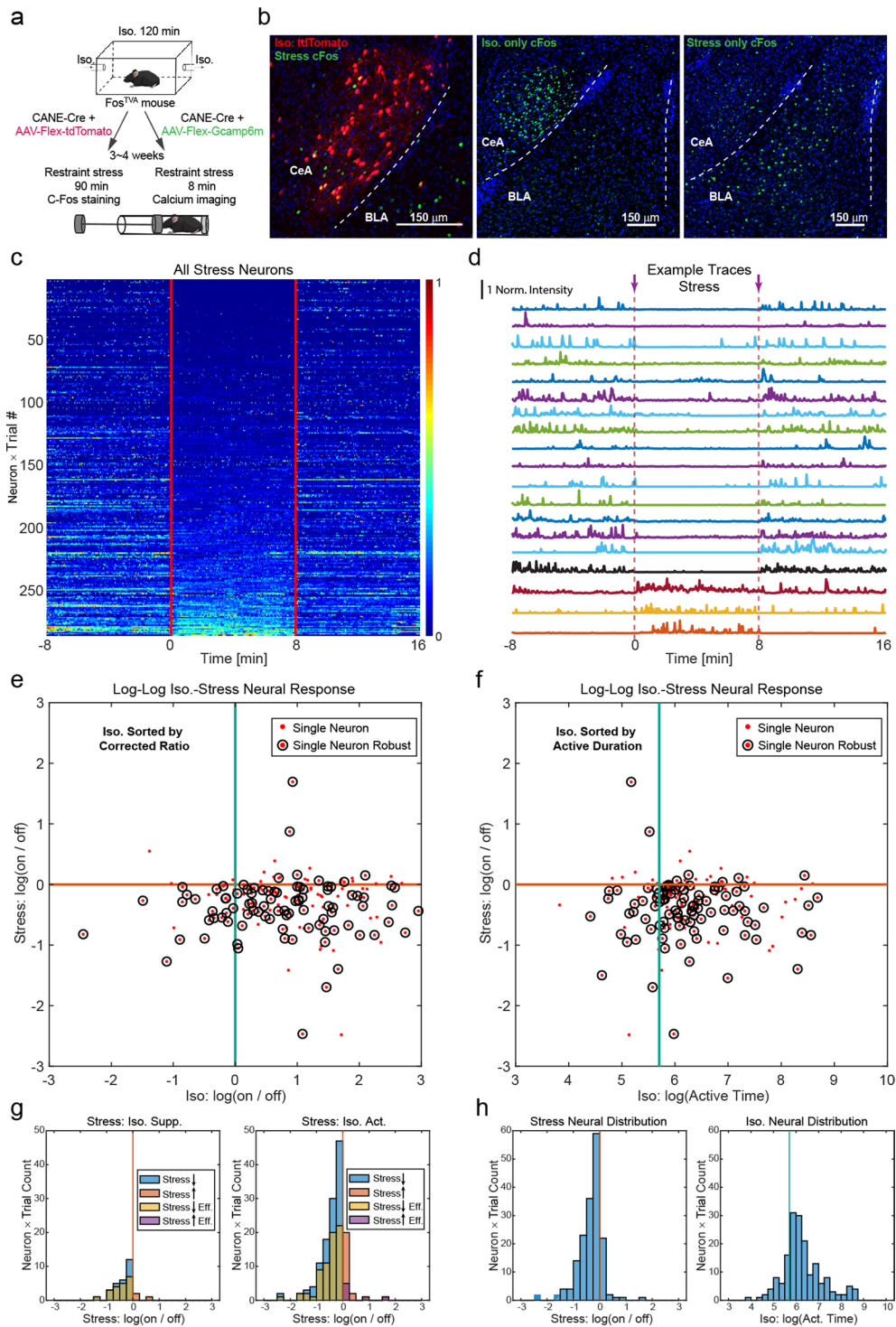


**Extended Data Fig. 1 | Isoflurane general anesthesia activates different neuronal ensembles and molecular marker analysis of CeA<sub>GA</sub> neurons.** General anesthesia activated the **a**, central amygdala (CeA), **b**, bed nucleus of stria terminalis (BNST), and **c**, super optic nucleus (SON). Representative images two-color experiments examining the expression of various markers in Fos+ CeA<sub>GA</sub> neurons (induced by isoflurane). **d**, CeA<sub>GA</sub> neurons are a subset of GABAergic (vGAT) neurons in the central amygdala and all CeA<sub>GA</sub> express vGAT-GFP. **e–i**, CeA<sub>GA</sub> neurons have minimal to no overlap with **e**, somatostatin (SST), **f**, prodynorphin (Pdyn), **g**, neurotensin (NTS), and **h, i**, calcitonin gene-related peptide receptor (CGRPR) expressing neurons in CeA.



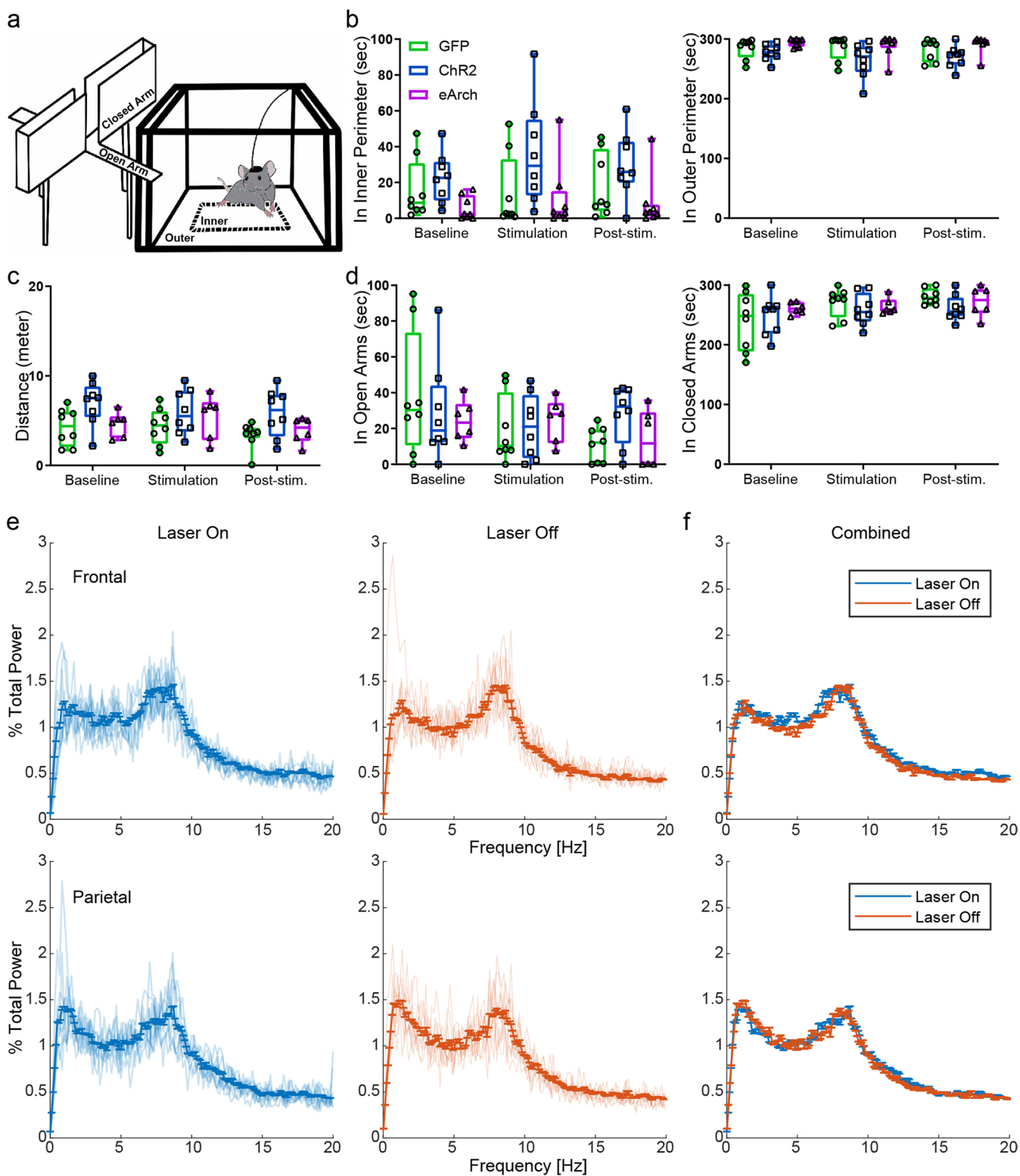
Extended Data Fig. 2 | See next page for caption

**Extended Data Fig. 2 | Representative post hoc histology and session distributions of activity of CANE-captured isoflurane-activated CeA<sub>CA</sub> neurons in response to isoflurane or ketamine.** **a**, Representative images of CANE-GCaMP6m+ neurons (green) and isoflurane-activated Fos<sup>+</sup> neurons (red) and their overlap. Dotted box showing the placement of the GRIN lens in CeA. **b**, Quantification of the percent colocalization of Iso:Fos&GCaMP6m:GFP/all GCaMP6m ( $75.45 \pm 5.04\%$ ) and Iso:Fos&GCaMP6m:GFP/all Fos ( $50.1 \pm 8.70\%$ ) ( $n = 6$  animals). Data are mean  $\pm$  s.e.m. **c**, Three consecutive representative images of post hoc histology showing optic fiber tract into the CeA from bregma  $-1.00$  mm to  $-1.16$  mm. Optic fiber diameter is  $200 \mu\text{m}$ . **d**, Session-wise percentage distribution of iso.-sustained and iso.-transient neurons from Fig. 2d. **e**, Session-wise percentage distribution of ketamine-sustained and ketamine-transient neurons from Fig. 2f. **f, g**, Session-wise percentage distribution of the isoflurane-activated neurons (**f**), or the ketamine-activated neurons (**g**), calculated using four methods calculated based on the ratio between the post- and pre-stimulation (that is anesthetic administration) activity. Cyan, Eff./Eff., mean activity of (post-stim) effective time / mean activity of (pre-stim) effective time. Orange, Mean/Mean, mean activity of all the (post-stim) time / mean activity of all the (pre-stim) time. Yellow, Eff./Mean, mean activity of (post-stim) effective time / mean activity of all the (pre-stim) time. Purple, Eff. time, total (post-stim) effective time. “Effective time” refers to the time points of a neural trace whose intensity is two median absolute deviation above its mean. Only these time points were considered to compute the effective mean. See Methods for details of the 4 methods. Pre-, pre-stimuli, awake state ( $-4-0$  min). Post-, post-stimuli, isoflurane or ketamine ( $0-20$  min).



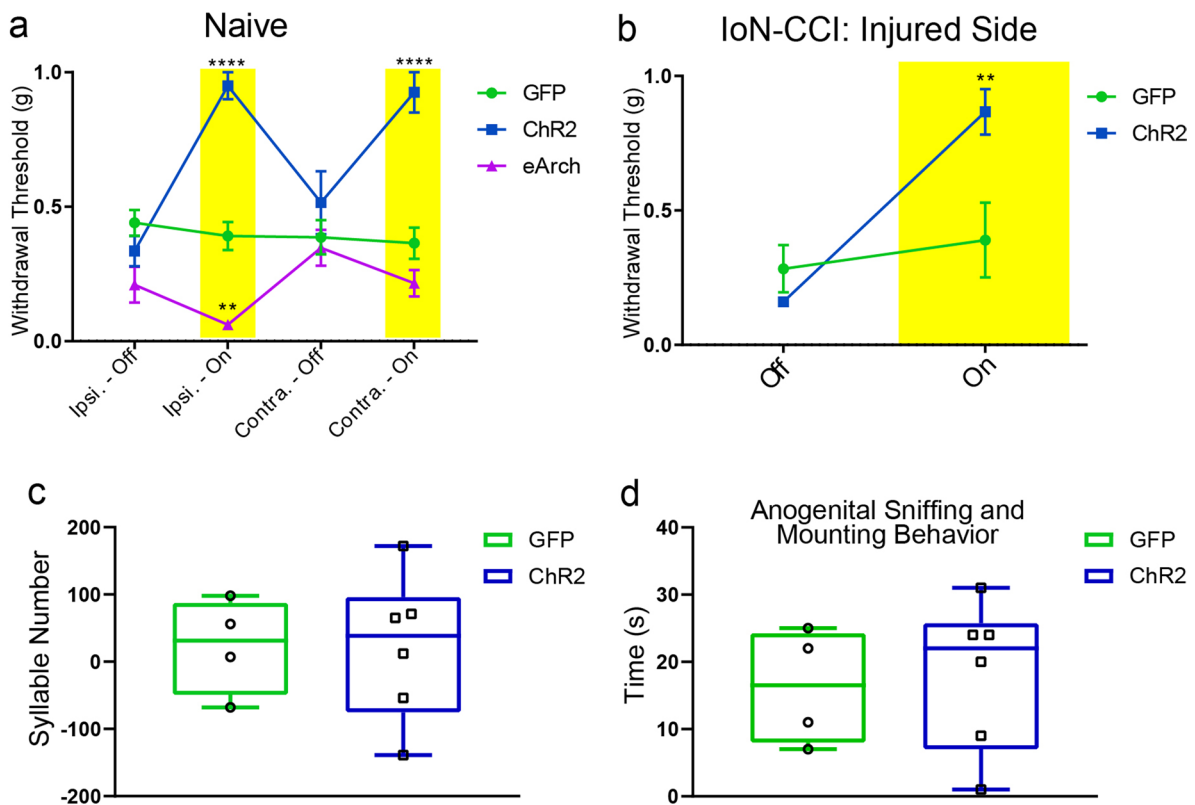
Extended Data Fig. 3 | See next page for caption

**Extended Data Fig. 3 | CANE-captured CeA<sub>GA</sub> neurons are mostly inhibited by stress.** **a**, Schematic of CANE captured *isoflurane*-activated CeA<sub>GA</sub> neurons followed by a second exposure to restraint stress (left, for Fos expression, right, for calcium imaging). **b**, Left, representative images of CANE<sub>ISO</sub>-tdTomato neurons (red) and stress-activated Fos<sup>+</sup> neurons (green) and their overlap. (n=3 animals). Right, representative images of isoflurane-only activated Fos<sup>+</sup> neurons (green, repeated experiments n=5 biologically independent samples.) and compared to stress-only activated Fos<sup>+</sup> neurons (green, repeated experiments n=3 biologically independent samples.) in the CeA. **c**, Heatmap, activity patterns of CANE<sub>ISO</sub>-GCaMP6m captured CeA<sub>GA</sub> neurons in stress experiment sorted by the average activity during stress period (-8-0 min, pre-stress; 0-8 min, restraint stress; 8-16 min, post-stress. 282 neurons from 5 mice × 2 trials). A small number of neurons (in the bottom of the heatmap) were activated by stress. **d**, Example traces of CANE<sub>ISO</sub>-GCaMP6m captured CeA<sub>GA</sub> neurons in stress experiment showing both stress-inhibited and stress-activated neurons. Norm. intensity: normalized calcium signals rescaled to 0-1. **e**, Scatter plots of the tracked same neurons based on isoflurane and stress related activity patterns. Each dot is calculated based on effectiveness corrected activity ratio between the post- and pre-stimulus periods for isoflurane-stimulus and stress-stimulus, separately. Corrected ratio, mean activity of (post-) effective time / mean activity of (pre-) effective time. Single dots represent individual neurons in the logarithmic scale coordinates, and the circled dots represent robustly firing neurons, with the maximum intensity of each neuron in the whole duration exceeding a threshold. **f**, Same plots with isoflurane responses calculated by actively firing time exceeding a threshold (1 min). Active duration, total (post-) effective time of effective moment >1 min. "Effective time" refers to the time points of a neural trace whose intensity is two median absolute deviation above its mean. Only these time points were considered to compute the mean. **g**, Neuron count summary of **e**. Left, Neuron count distribution of activity of isoflurane-suppressed neurons during stress. Right, Neural count distribution of activity of isoflurane-activated neurons during stress. **h**, Neural count distribution of **f**. Left, marginal count distribution of activity of CANE<sub>ISO</sub>-GCaMP6m captured CeA<sub>GA</sub> neurons during stress. Right, marginal count distribution of activity of CANE<sub>ISO</sub>-GCaMP6m captured CeA<sub>GA</sub> neurons during isoflurane GA.



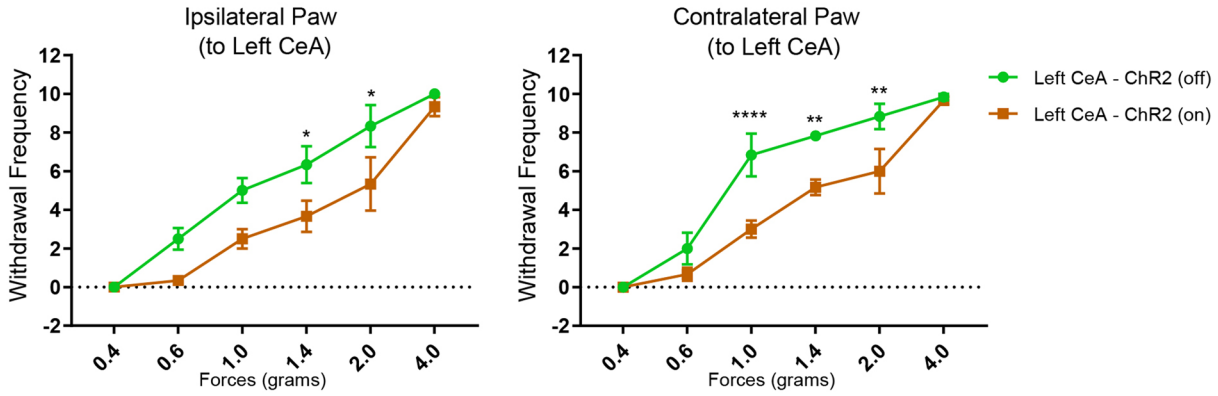
Extended Data Fig. 4 | See next page for caption

**Extended Data Fig. 4 | Manipulation of CeA<sub>GA</sub> neurons did not induce anxiety-like or fear-like behavior or change the gross brain state. a**, Schematics of the Elevated Plus Maze (left) and Open Field (right) apparatus. **b**, Quantification of total time spent in the inner (GFP:  $15.67 \pm 5.97$  s (baseline),  $14.18 \pm 7.24$  s (stim),  $18.07 \pm 6.38$  s (post)); ChR2:  $22.59 \pm 4.92$  s (baseline),  $35.90 \pm 10.22$  s (stim),  $29.73 \pm 6.49$  s (post); eArch:  $5.69 \pm 2.32$  s (baseline),  $11.01 \pm 6.61$  s (stim),  $8.54 \pm 5.20$  s (post)) and outer perimeter (GFP:  $284.32 \pm 6.01$  s (baseline),  $285.70 \pm 7.25$  s (stim),  $281.80 \pm 6.39$  s (post); ChR2:  $277.31 \pm 4.92$  s (baseline),  $264.00 \pm 10.22$  s (stim),  $270.17 \pm 6.47$  s (post); eArch:  $294.31 \pm 2.32$  s (baseline),  $288.99 \pm 6.61$  s (stim),  $291.46 \pm 5.20$  s (post)) of the Open Field Test (control,  $n=8$  animals, ChR2,  $n=8$  animals, eArch,  $n=6$  animals; two-way repeated measures ANOVA;  $P$ -value was above 0.05, no significance;  $F_{4,42}=0.8743$  (inner),  $F_{4,42}=0.8633$  (outer)). Data are mean  $\pm$  s.e.m. **c**, Quantification of total distance travelled (GFP:  $4.27 \pm 0.73$  m (baseline),  $4.36 \pm 0.72$  m (stim),  $3.36 \pm 0.51$  m (post)); ChR2:  $6.92 \pm 0.87$  m (baseline),  $5.91 \pm 0.88$  m (stim),  $5.85 \pm 0.95$  m (post); eArch:  $4.59 \pm 0.56$  m (baseline),  $5.45 \pm 0.99$  m (stim),  $3.91 \pm 0.59$  m (post)), and **d**, total time spent in the open (GFP:  $38.53 \pm 12.26$  s (baseline),  $19.19 \pm 6.65$  s (stim),  $11.03 \pm 3.44$  s (post); ChR2:  $28.61 \pm 9.69$  s (baseline),  $21.21 \pm 6.31$  s (stim),  $27.91 \pm 5.76$  s (post); eArch ( $24.33 \pm 4.70$  s (baseline),  $24.85 \pm 4.98$  s (stim),  $14.35 \pm 6.56$  s (post)) and closed arms (GFP:  $239.16 \pm 17.28$  s (baseline),  $270.86 \pm 8.54$  s (stim),  $280.76 \pm 4.61$  s (post); ChR2:  $248.58 \pm 11.66$  s (baseline),  $258.80 \pm 9.36$  s (stim),  $261.08 \pm 7.60$  s (post); eArch ( $261.22 \pm 4.07$  s (baseline),  $264.45 \pm 5.50$  s (stim),  $272.48 \pm 10.19$  s (post)) of the Elevated Plus Maze (control,  $n=8$  animals, ChR2,  $n=8$  animals, eArch,  $n=8$  animals; two-way repeated measures ANOVA;  $P$ -value was above 0.05, no significance;  $F_{4,38}=1.083$  (distance),  $F_{4,38}=1.402$  (open arms),  $F_{4,38}=1.355$  (closed arms)). Data are mean  $\pm$  s.e.m. **e**, Power spectrum of EEG signals in the frontal and parietal cortex. Left, laser on, right, laser off. **f**, Overlap of power spectrum of EEG signals in the frontal and parietal cortex from **e**. The mean spectrum in each condition was calculated from the average across 9 sessions ( $n=3$  mice, 2 min laser on / 2 min laser off, 3 repetitions in each mouse). The error bar represents the standard error. The power spectrum was normalized.

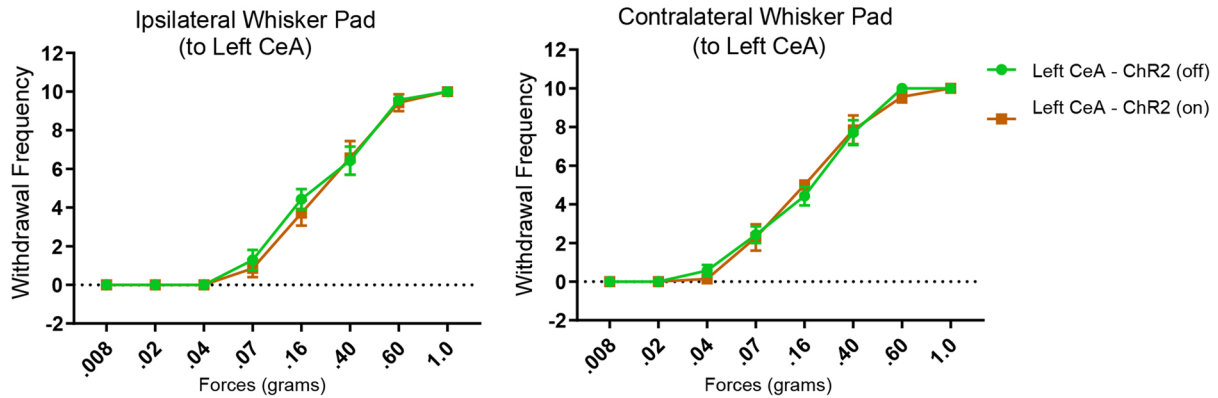


**Extended Data Fig. 5 | Manipulations of CeA<sub>GA</sub> neurons modulated reflexive withdrawal threshold to von Frey filaments and activation of CeA<sub>GA</sub> neurons did not alter courtship behaviors.** **a, b**, Quantifications of the withdrawal threshold to von Frey filaments applied to the whisker pad in **a**, naive (control,  $n = 9$  animals ( $0.44 \pm 0.05$  (ipsi-off),  $0.39 \pm 0.05$  (ipsi-on),  $0.39 \pm 0.06$  (contra-off),  $0.36 \pm 0.06$  (contra-on)), ChR2,  $n = 8$  animals ( $0.34 \pm 0.06$  (ipsi-off),  $0.95 \pm 0.05$  (ipsi-on),  $0.52 \pm 0.12$  (contra-off),  $0.93 \pm 0.08$  (contra-on)), eArch,  $n = 7$  animals ( $0.21 \pm 0.07$  (ipsi-off),  $0.06 \pm 0.01$  (ipsi-on),  $0.35 \pm 0.07$  (contra-off),  $0.22 \pm 0.05$  (contra-on)); two-way ANOVA; \*\*\*\* $P < 0.0001$ , \*\* $P = 0.0042$ ;  $F_{6,84} = 10.80$ ) and **b**, loN-CCI mice (control,  $n = 6$  animals ( $0.28 \pm 0.09$  (off),  $0.39 \pm 0.14$  (on)), ChR2,  $n = 6$  animals ( $0.16 \pm 0.0$  (off),  $0.87 \pm 0.08$  (on)); two-way ANOVA; \*\* $P = 0.0032$ ;  $F_{1,20} = 10.54$ ). **c-d**, Quantification of light-illumination induced changes in total syllable number of ultrasonic vocalizations (GFP:  $23.25 \pm 35.65$ ; ChR2:  $21.17 \pm 44.17$ ), or total duration of anogenital sniffing and mounting behavior (GFP:  $16.25 \pm 4.31$ ; ChR2:  $18.17 \pm 4.53$  s) in control CeA<sub>GA</sub>-GFP and CeA<sub>GA</sub>-ChR2 mice (with light - without light) during 2 min of social interactions (control,  $n = 4$  animals, ChR2,  $n = 6$  animals; unpaired t-test, two-tailed;  $P = 0.974$ ,  $F_{5,3} = 2.303$  (syllable number),  $P = 0.7791$ ,  $F_{5,3} = 1.656$  (anogenital sniffing)). Data are mean  $\pm$  s.e.m.

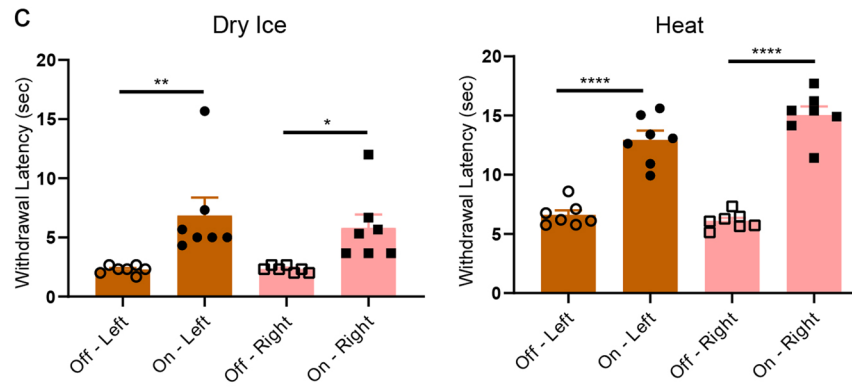
**a** Von Frey - Paw



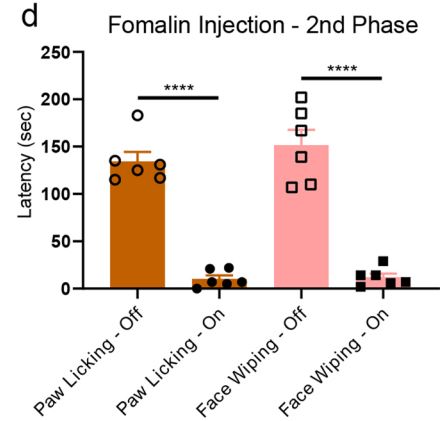
**b** Von Frey - Whisker Pad



**c**

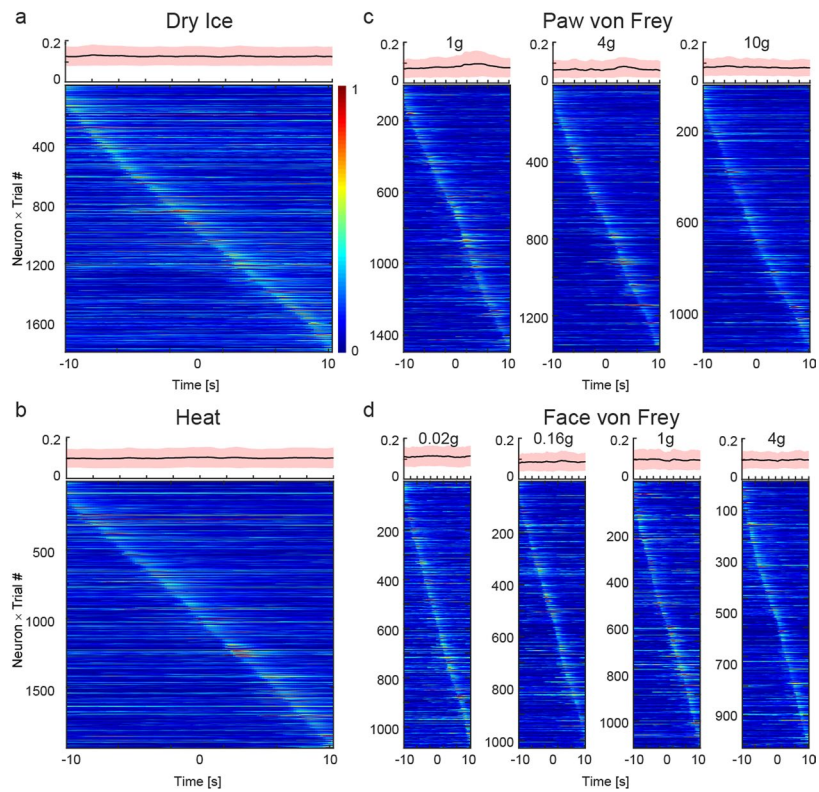


**d**

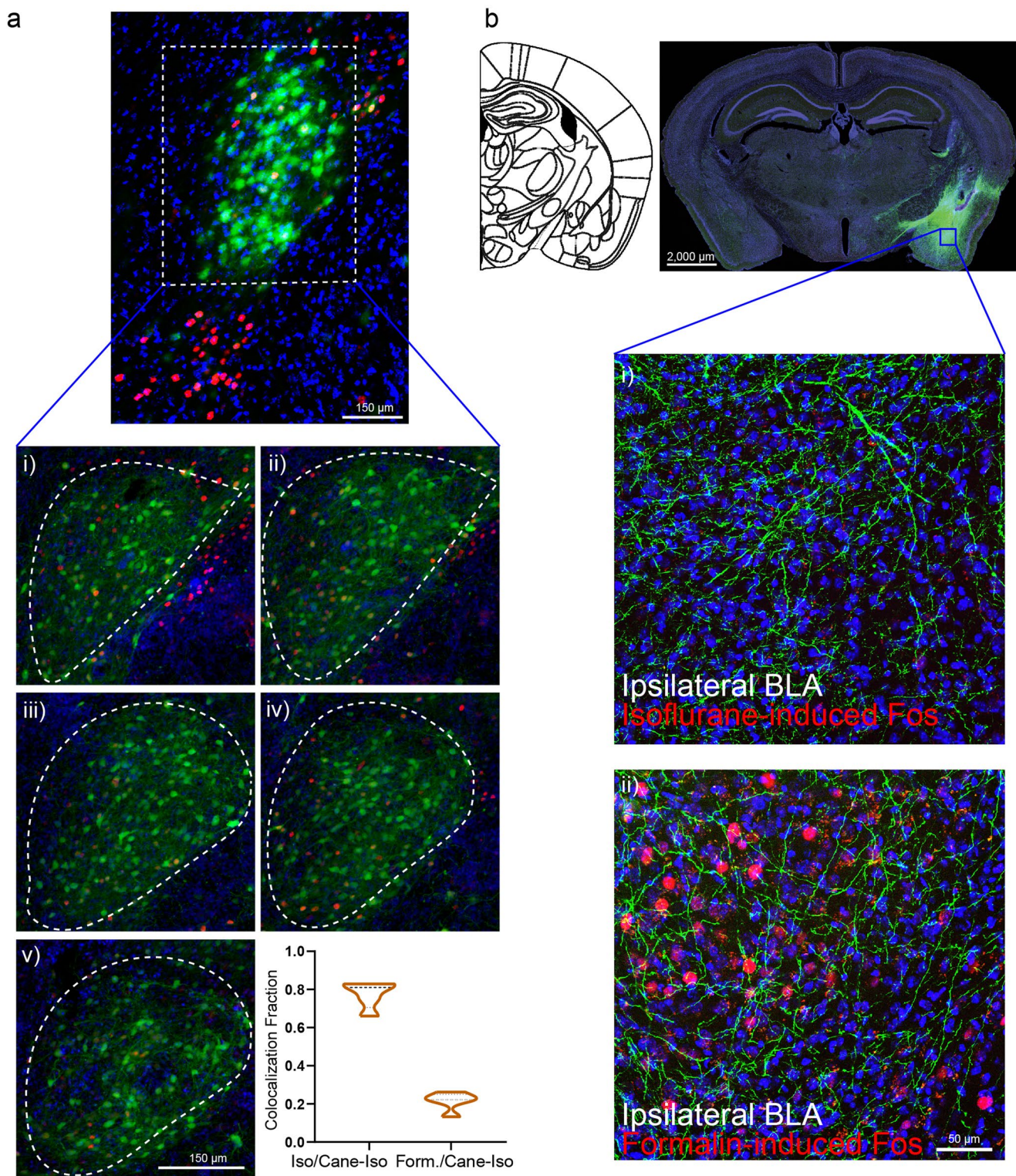


Extended Data Fig. 6 | See next page for caption

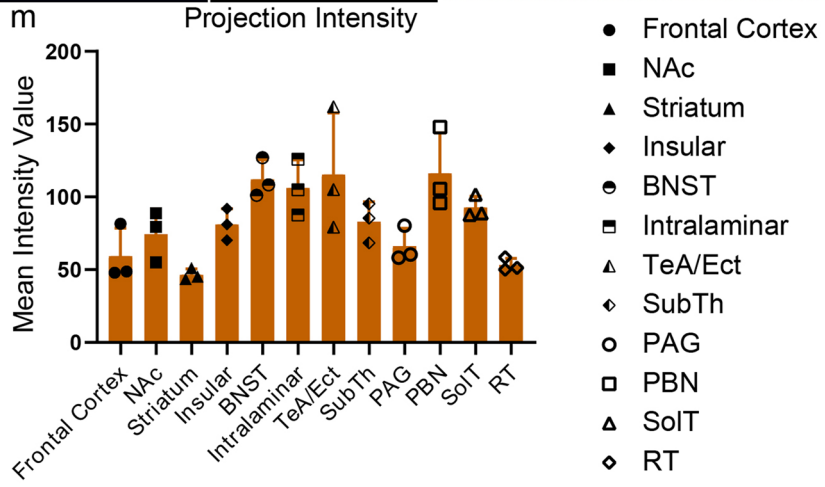
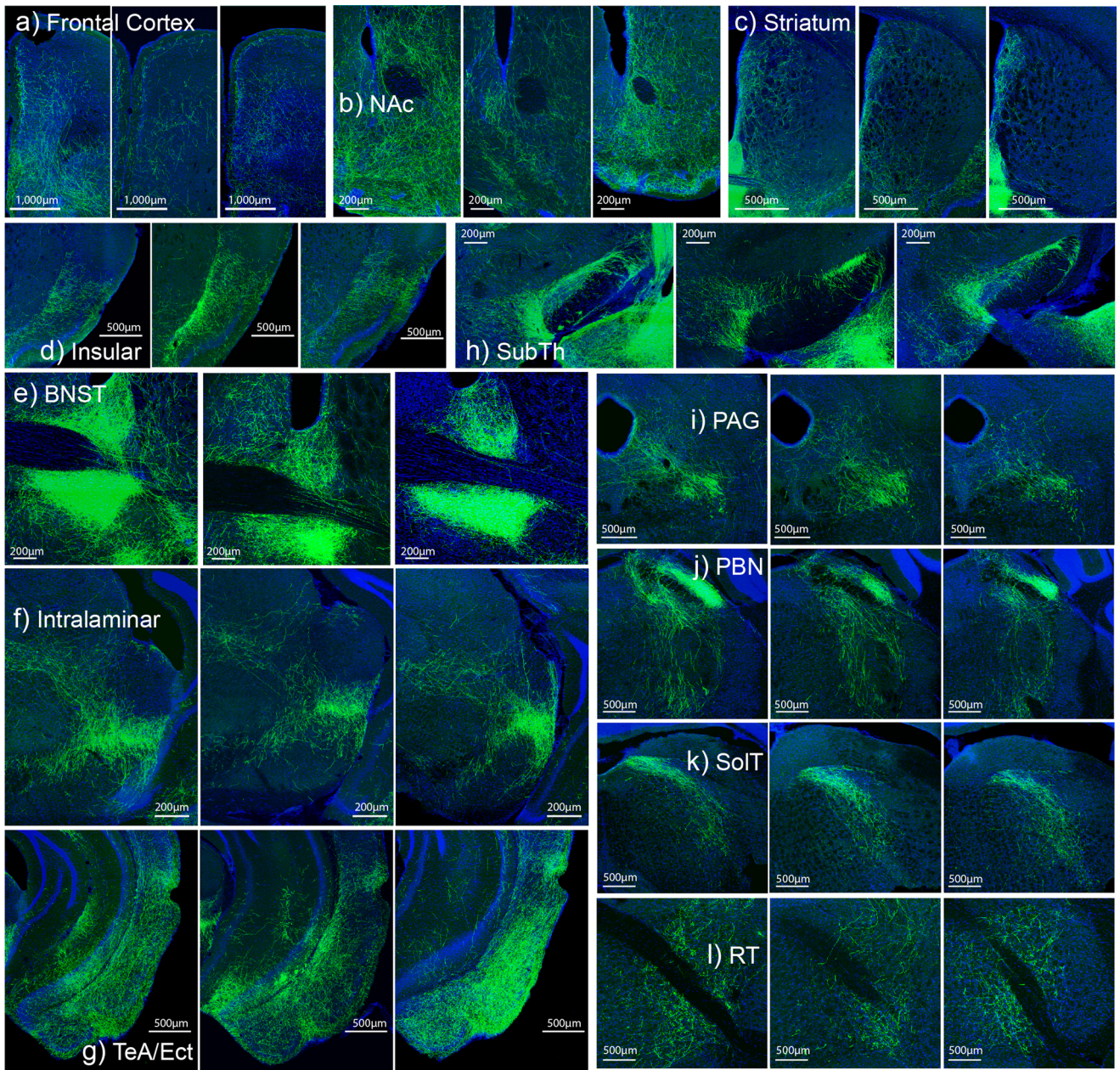
**Extended Data Fig. 6 | Activation of the left CeA<sub>GA</sub> neurons modulated pain-related behaviors in naïve mice and acute pain models. a.** Quantification of effects of optogenetic activation of the left CeA<sub>GA</sub> neurons on the paw withdrawal frequency to six graded von Frey filaments ranging from 0.4 to 4.0 grams applied to the ipsilateral (Off:  $0 \pm 0$  (0.40g),  $2.50 \pm 0.56$  (0.60g),  $5.00 \pm 0.63$  (1.0g),  $6.33 \pm 0.95$  (1.40g),  $8.33 \pm 1.09$  (2.0g),  $10 \pm 0$  (4.0g); On:  $0 \pm 0$  (0.40g),  $0.33 \pm 0.21$  (0.60g),  $2.50 \pm 0.50$  (1.0g),  $3.67 \pm 0.80$  (1.40g),  $5.33 \pm 1.38$  (2.0g),  $9.33 \pm 0.49$  (4.0g)) or contralateral paw (Off:  $0 \pm 0$  (0.40g),  $2.00 \pm 0.82$  (0.60g),  $6.83 \pm 1.11$  (1.0g),  $7.83 \pm 0.17$  (1.40g),  $8.83 \pm 0.65$  (2.0g),  $9.83 \pm 0.17$  (4.0g); On:  $0 \pm 0$  (0.40g),  $0.67 \pm 0.33$  (0.60g),  $3.00 \pm 0.45$  (1.0g),  $5.0 \pm 0.37$  (1.40g),  $6.0 \pm 1.15$  (2.0g),  $9.67 \pm 0.21$  (4.0g)) to the left CeA. (Ipsilateral and contralateral, ChR2, n=6 animals; two-way ANOVA; \*P=0.0500 (2.0g), \*P=0.0217 (1.4g), \*\*\*\*P<0.0001, \*\*P=.0023 (1.4g), \*\*P=.0029 (2.0g);  $F_{1,60}=20.51$  (ipsi),  $F_{1,60}=28.81$  (contra)). **b.** Quantification of optogenetic activation of the left CeA<sub>GA</sub> neurons showed that this manipulation did not induce any change in the head withdrawal frequency to eight von Frey filaments ranging from 0.008 to 1.0 gram applied to either the ipsilateral (Off:  $0 \pm 0$  (0.008g),  $0 \pm 0$  (0.02g),  $0 \pm 0$  (0.04g),  $1.0 \pm 0.52$  (0.07g),  $4.33 \pm 0.61$  (0.16g),  $6.50 \pm 0.85$  (0.40g),  $9.67 \pm 0.21$  (0.60g),  $10.0 \pm 0$  (1.0g); On:  $0 \pm 0$  (0.008g),  $0 \pm 0$  (0.02g),  $0 \pm 0$  (0.04g),  $0.67 \pm 0.49$  (0.07g),  $4.17 \pm 0.54$  (0.16g),  $7.00 \pm 0.89$  (0.40g),  $9.83 \pm 0.17$  (0.60g),  $10.0 \pm 0$  (1.0g)) or the contralateral whisker pad (Off:  $0 \pm 0$  (0.008g),  $0 \pm 0$  (0.02g),  $0.50 \pm 0.34$  (0.04g),  $2.50 \pm 0.50$  (0.07g),  $4.67 \pm 0.49$  (0.16g),  $8.0 \pm 0.68$  (0.40g),  $10.0 \pm 0$  (0.60g),  $10.0 \pm 0$  (1.0g); On:  $0 \pm 0$  (0.008g),  $0 \pm 0$  (0.02g),  $0.17 \pm 0.17$  (0.04g),  $2.33 \pm 0.80$  (0.07g),  $5.17 \pm 0.17$  (0.16g),  $8.17 \pm 0.79$  (0.40g),  $9.83 \pm 0.17$  (0.60g),  $10.0 \pm 0$  (1.0g)) to the left CeA. (Ipsilateral and contralateral, ChR2, n=6 animals; two-way ANOVA; not significant  $P > 0.05$ ;  $F_{1,80}=0.9205$  (ipsi),  $F_{1,40}=0.000$  (contra)). **c.** Quantification of the optogenetics induced changes in withdrawal latency (sec) to dry ice ( $2.29 \pm 0.33$  s (off-left),  $6.86 \pm 3.70$  s (on-left),  $2.33 \pm 0.25$  s (off-right),  $5.81 \pm 2.75$  s (on-right)) (ChR2, n=7 animals; one-way ANOVA; \*\*P=0.0045, \*P=0.0311;  $F_{3,24}=6.241$ ) and heat ( $6.61 \pm 0.93$  s (off-left),  $12.94 \pm 1.89$  s (on-left),  $6.09 \pm 0.65$  s (off-right),  $15.04 \pm 1.80$  s (on-right)) (ChR2, n=7 animals; one-way ANOVA; \*\*\*\*P<0.0001;  $F_{3,24}=59.93$ ). **d.** Quantification of total licking and face wiping latency (sec) from left CeA<sub>GA</sub> neurons optogenetic activation after formalin injection during the second phase of inflammatory pain ( $134.33 \pm 22.88$  s (paw licking-off),  $10.33 \pm 8.24$  s (paw licking-on),  $151.67 \pm 35.99$  s (face wiping-off),  $12.00 \pm 8.74$  s (face wiping-on)). (ChR2, n=6 animals; one-way ANOVA; \*\*\*\*P<0.0001;  $F_{3,20}=59.54$ ).



**Extended Data Fig. 7 |  $\text{CeA}_{\text{GA}}$  activities are not correlated to the onsets of sensory stimuli.** Neuronal activity patterns during **a**, cold, **b**, heat, **c**, paw von Frey, and **d**, face von Frey tests sorted by neurons peak responses timing: from -10 to +10 sec, with 0 as the onset of stimulus application. Top of each heatmap, averaged population activity from 10 seconds before to 10 seconds after each stimulus onset. Thick lines indicated mean and shaded areas indicated s.e.m.

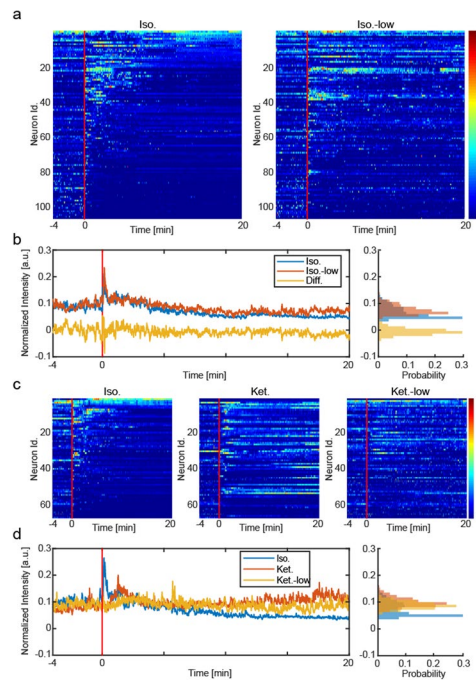


**Extended Data Fig. 8 | CeA<sub>GA</sub> neurons are distinct from pain-activated neurons in CeA and high magnification image of CeA<sub>GA</sub> neurons projection into the ipsilateral BLA.** **a**, CeA<sub>GA</sub> neurons have minimal co-localization with formalin-induced Fos+ cells. Formalin-activated cells primarily locate in the capsular division of CeA outside the lateral division where CeA<sub>GA</sub> locate. Insert **i-v**), Example of five consecutive slices of the lateral division of CeA showing minimal co-localization with formalin-induced Fos+ cells with CeA<sub>GA</sub> neurons, and the quantification of fraction of co-localization between CANE-captured CeA<sub>GA</sub> cells and formalin-induced Fos+ cells ( $n=5$  biologically independent samples for each condition) ( $0.78 \pm 0.06$  (Iso/Cane-Iso);  $0.22 \pm 0.04$  (Form./Cane-Iso)). **b**, Coronal schematic next to example coronal slice of low magnification (high exposure) of CANE-GFP labeled CeA<sub>GA</sub> neurons and their axons with a box around the ipsilateral BLA. Insert **i-ii**), High mag images show projections in ipsilateral BLA with top panel showing that isoflurane did not induce Fos+ cells, and bottom panel showing that formalin-pain induced robust Fos+ expression in BLA. ( $n=3$  biologically independent samples).



Extended Data Fig. 9 | See next page for caption

**Extended Data Fig. 9 | Consistent axonal projections from CeA<sub>CA</sub> neurons.** In sequential order: **a**, frontal cortex, **b**, nucleus accumbens (NAc), **c**, striatum, **d**, insular, **e**, bed nucleus stria terminalis (BNST), **f**, intralaminar, **g**, temporal association cortex (TeA) and ectorhinal cortex (Ect), **h**, subthalamic nucleus (SubTh), **i**, periaqueductal grey (PAG), **j**, parabrachial nucleus (PBN), **k**, solitary tract (SolT), and **l**, reticular formation (RT). **m**, Quantification of the mean intensity value (artificial units) of the axonal projections from each region of interest (ROI) listed above (**a-l**) ( $n=3$  biologically independent samples) ( $59.40 \pm 15.68$  (FC),  $74.38 \pm 14.18$  (NAc),  $46.59 \pm 3.21$  (Striatum),  $81.07 \pm 8.86$  (Ins),  $112.09 \pm 10.85$  (BNST),  $106.15 \pm 15.69$  (Intra),  $115.35 \pm 34.52$  (TeA/Ect),  $82.99 \pm 11.06$  (SubTh),  $66.32 \pm 9.84$  (PAG),  $116.29 \pm 22.67$  (PBN),  $92.70 \pm 6.27$  (SolT),  $53.26 \pm 3.63$  (RT)).



**Extended Data Fig. 10 | CeA<sub>GA</sub> neurons are also activated by low dose anesthetics.** **a**, Heatmaps, activity patterns of the same neurons tracked in isoflurane (1.5%) and low isoflurane (0.5%) experiments, aligned by isoflurane (1.5%) neural patterns. 106 tracked same neurons from 5 mice  $\times$  1 trial. **b**, Left, mean and difference traces of the population normalized activity in isoflurane and low isoflurane experiments. Right, intensity distribution of the traces. **c**, Heatmaps, activity patterns of the same neurons tracked in isoflurane (1.5%), ketamine (100 mg/kg) and low ketamine (12 mg/kg) experiments, aligned by isoflurane neural patterns. 69 tracked same neurons from 5 mice  $\times$  1 trial. **d**, Left, mean trace of the population normalized activity in isoflurane, ketamine and low ketamine experiments. Right, intensity distribution of the traces.

## Reporting Summary

Nature Research wishes to improve the reproducibility of the work that we publish. This form provides structure for consistency and transparency in reporting. For further information on Nature Research policies, see [Authors & Referees](#) and the [Editorial Policy Checklist](#).

### Statistics

For all statistical analyses, confirm that the following items are present in the figure legend, table legend, main text, or Methods section.

n/a Confirmed

- The exact sample size ( $n$ ) for each experimental group/condition, given as a discrete number and unit of measurement
- A statement on whether measurements were taken from distinct samples or whether the same sample was measured repeatedly
- The statistical test(s) used AND whether they are one- or two-sided  
*Only common tests should be described solely by name; describe more complex techniques in the Methods section.*
- A description of all covariates tested
- A description of any assumptions or corrections, such as tests of normality and adjustment for multiple comparisons
- A full description of the statistical parameters including central tendency (e.g. means) or other basic estimates (e.g. regression coefficient) AND variation (e.g. standard deviation) or associated estimates of uncertainty (e.g. confidence intervals)
- For null hypothesis testing, the test statistic (e.g.  $F$ ,  $t$ ,  $r$ ) with confidence intervals, effect sizes, degrees of freedom and  $P$  value noted  
*Give  $P$  values as exact values whenever suitable.*
- For Bayesian analysis, information on the choice of priors and Markov chain Monte Carlo settings
- For hierarchical and complex designs, identification of the appropriate level for tests and full reporting of outcomes
- Estimates of effect sizes (e.g. Cohen's  $d$ , Pearson's  $r$ ), indicating how they were calculated

*Our web collection on [statistics for biologists](#) contains articles on many of the points above.*

### Software and code

Policy information about [availability of computer code](#)

Data collection: AnyMaze Software 6.0; Inscopix nVista 3.0

Data analysis: GraphPad Prism 8; MatLab and MIN1PIPE available via GitHub

For manuscripts utilizing custom algorithms or software that are central to the research but not yet described in published literature, software must be made available to editors/reviewers. We strongly encourage code deposition in a community repository (e.g. GitHub). See the Nature Research [guidelines for submitting code & software](#) for further information.

### Data

Policy information about [availability of data](#)

All manuscripts must include a [data availability statement](#). This statement should provide the following information, where applicable:

- Accession codes, unique identifiers, or web links for publicly available datasets
- A list of figures that have associated raw data
- A description of any restrictions on data availability

All raw data described in this study are available from the corresponding authors upon request. All codes described in this study are available from the corresponding authors upon request. The MIN1PIPE code is processing miniscope imaging (correspondence should be addressed to Jinghao Lu, [jinghao.lu@duke.edu](mailto:jinghao.lu@duke.edu)) is available at: <https://github.com/JinghaoLu/MIN1PIPE>

### Field-specific reporting

Please select the one that best describes your research. If you are not sure, read the appropriate sections before making your selection.

- Life sciences
- Behavioural & social sciences
- Ecological, evolutionary & environmental sciences

For a reference copy of the document with all sections, see [nature.com/documents/nr-reporting-summary-flat.pdf](https://nature.com/documents/nr-reporting-summary-flat.pdf)

# Life sciences study design

All studies must disclose on these points even when the disclosure is negative.

|                 |   |
|-----------------|---|
| Sample size     | Sample sizes were determined based on previous publications and common practice in animal behavior experiments.   |
| Data exclusions | During post-hoc immunohistochemistry, viral expression, site of injection and insertion of optical fiber was confirmed; animals with failed expression or off target optical fiber placement were excluded from all analysis.   |
| Replication     | Experimental findings were reliably reproduced among all subjects in all experiments comprised of multiple cohorts. Indication of each subject was indicted in all figures when possible. This is reported throughout the figure legends and Methods to ensure reproducibility. |
| Randomization   | Animals were randomly selected from each litter. Random group allocation was maintained throughout the study, within constraints set by availability of in-house, purpose-bred lines.   |
| Blinding        | Investigators were blinded to group allocation during data analysis.  |

## Reporting for specific materials, systems and methods

We require information from authors about some types of materials, experimental systems and methods used in many studies. Here, indicate whether each material, system or method listed is relevant to your study. If you are not sure if a list item applies to your research, read the appropriate section before selecting a response.

### Materials & experimental systems

### Methods

| n/a                                 | Involved in the study   | n/a                                 | Involved in the study                           |
|-------------------------------------|---|-------------------------------------|---|
| <input type="checkbox"/>            | <input checked="" type="checkbox"/> Antibodies                  | <input checked="" type="checkbox"/> | <input type="checkbox"/> ChIP-seq               |
| <input checked="" type="checkbox"/> | <input type="checkbox"/> Eukaryotic cell lines                  | <input checked="" type="checkbox"/> | <input type="checkbox"/> Flow cytometry         |
| <input checked="" type="checkbox"/> | <input type="checkbox"/> Palaeontology                          | <input checked="" type="checkbox"/> | <input type="checkbox"/> MRI-based neuroimaging |
| <input type="checkbox"/>            | <input checked="" type="checkbox"/> Animals and other organisms |                                     |   |
| <input checked="" type="checkbox"/> | <input type="checkbox"/> Human research participants            |                                     |   |
| <input checked="" type="checkbox"/> | <input type="checkbox"/> Clinical data                          |                                     |   |

## Antibodies

|                 |  |
|-----------------|--|
| Antibodies used | goat anti-Fos (Santa Cruz Biotechnology, sc520g, 1:300)(Venza, M. et al, 2015), anti-Neurotensin (ImmunoStar, 20072, 1:1000)(Faget, L. et al, 2018), Alexa Fluor 488 donkey anti-goat (Jackson ImmunoResearch, 705-545-147, 1:500)(Zamparo, I. et al, 2019), and Cy3 donkey anti-goat (Jackson ImmunoResearch, 705-165-147, 1:500)(Simon, C.M. et al, 2019), rabbit anti-Fos (Cell Signaling, #2250, 1:1500)(Pang, D. et al, 2020), Alexa Fluor 647 anti-rabbit (Jackson ImmunoResearch, 711-605-152: 1:1500)(Hara, Y. et al, 2020).   |
| Validation      | The antibodies were validated by their respective companies (as mentioned above) by Western blot and were used widely by many publications. Furthermore, the anti-Fos antibody results presented in this study were validated by two color fluorescence in situ hybridization with Fos RNA probe. The species are as mentioned above such as "goat, rabbit, donkey" and application was for immunohistochemistry and free floating hybridization chain reaction. For specific citations, please refer to information in "antibodies used" above and for each antibody, we cited a reference in the manuscript. |

## Animals and other organisms

Policy information about [studies involving animals](#); [ARRIVE guidelines](#) recommended for reporting animal research

|                         |  |
|-------------------------|--|
| Laboratory animals      | Adult (>8 weeks old) male and female FosTVA knock-in mice (JAX #027831) and adult vGAT-IRES-cre mice (JAX #016962) were used in this study. Animals were housed in standard 12h dark/12h light cycle at common facility and all experimental procedures were approved by Duke Animal Care and Use Program. |
| Wild animals            | The study did not involve any wild animals.  |
| Field-collected samples | The study did not involve any samples collected from the field.  |
| Ethics oversight        | All experiments were conducted according to protocols approved by The Duke University Institutional Animal Care and Use Committee.   |

Note that full information on the approval of the study protocol must also be provided in the manuscript.